Draft version March 12, 2009
Preprint typeset using LaTeX style emulateapj v. 08/13/06

MODES OF STAR FORMATION IN THE INTERACTING COMPACT GALAXY GROUP HCG 31: A HIGH REDSHIFT ANALOGUE?

S. C. Gallagher,[1,2] P. R. Durrell,[3] D. Elmegreen,[4] R. Chandar,[5] J. English,[6] J. C. Charlton,[7] C. Gronwall,[7] J. Young,[7] P. Tzanavaris,[8] K. E. Johnson,[9,10] M. de Oliveira,[11] B. Whitmore,[12] A. E. Hornschemeier,[8] et al.

Draft version March 12, 2009

ABSTRACT

The handful of late-type galaxies that comprise Hickson Compact Group 31 is in the midst of ongoing and complex gravitational interactions, evocative of the process of hierarchical structure formation at high redshift. We explore the accuracy of this analogy through the investigation of modes of star formation from compact, parsec scale clusters to kiloparsec scale complexes. With sensitive, multicolor *Hubble Space Telescope* imaging, we characterize the large population of <10 Myr old star clusters that suffuse the system. From the examination of young and globular star cluster systems, we find that HCG 31 is representative of other interacting, actively star-forming low-mass galaxies in the local Universe. However, in both the main galaxies and the tidal dwarf candidate F, stellar complexes (sensitive to the magnitude of disk turbulence) have both sizes and masses more characteristic of $z = 1$–2 galaxies. The low velocity dispersion of the system components, available reservoir of H I, and current star formation rate of $\sim 4\ \mathrm{M_\odot\ yr^{-1}}$, indicate that HCG 31 is likely to both exhaust its cold gas supply and merge within the next few Gyrs. We speculate that the end product will be a low-mass elliptical with an X-ray halo, a smaller version of the fossil groups found in the local Universe.

Subject headings: galaxies: star clusters — galaxies: interactions — galaxies: evolution — galaxies: clusters: individual (HCG 31)

1. INTRODUCTION

Massive elliptical galaxies are preferentially found in high density environments such as galaxy clusters – galaxy morphology and environment are clearly coupled in the local Universe (Dressler 1980). However, the mechanism for morphological transformation from star-forming and disk-dominated to quiescent and bulge-dominated is still uncertain. For example, is ram-pressure stripping important as a galaxy plows through the hot intracluster medium (ICM)? Alternatively, gravitational interactions from harassment to mergers might dominate the transformation process. Secular evolution whereby gas is sheparded inwards, thus triggering star formation and exhausting the material for subsequent generations of stars, could be important. The action of an active galactic nucleus (AGN) may also significantly alter its host in dense regions.

Furthermore, the question of *when* morphological transformation occurs in the hierarchical build-up of a galaxy cluster from subunits of galaxy groups is still open. Determining if galaxies are primarily processed while still contained within the unit of the group will shed light on the influence of the ICM, for example. Already, the demographics of cluster galaxies as a function of redshift indicate that this is occurring (e.g., Dressler et al. 1997). Studies of compact group galaxies offer the promise to further elucidate this issue, as they have the densities of galaxy clusters, but without (with a few exceptions) an X-ray emitting intragroup medium (IGM). The lower velocity dispersions ($\sigma \sim 10^2\ \mathrm{km\,s^{-1}}$) in groups compared to clusters ($\sigma \sim 10^3\ \mathrm{km\,s^{-1}}$) also prolong gravitational interactions. This context is relevant therefore for evaluating the role of gravitational interactions in morphological transformation before the cluster potential or ICM becomes dominant.

Recent *Spitzer* results on compact group galaxies suggest that the transformation from neutral gas-rich and actively star-forming to neutral gas-poor and quiescent can occur quite rapidly in this environment. Specifically, Johnson et al. (2007) found that most member galaxies in compact groups in an early evolutionary state (defined by a high ratio of their H I to dynamical masses) are actively star-forming as judged from their infrared luminosities and colors, while those with little H I are dominated by the stellar photospheric emission of old stellar populations. While this is perhaps not surprising, there is a notable gap in infrared properties of the compact group population compared to a sample of local galaxies matched in optical luminosity from the SINGS survey; the SINGS galaxies have a continuous distribution of infrared properties (Gallagher et al. 2008). The lack of compact group galaxies in the intermediate region of infrared color-space suggests that this location is crossed quickly (Johnson et al. 2007). This picture of galaxy processing in this environment is further demonstrated by the H I deficiency of late-type compact group galaxies relative to those in loose groups and the field (Williams & Rood 1987; Verdes-Montenegro et al. 2001).

[1] Department of Physics & Astronomy, The University of Western Ontario, London, ON, N6A 3K7, CANADA; *sgalla4@uwo.ca*
[2] Department of Physics & Astronomy, University of California – Los Angeles, Los Angeles CA, 90095–1547, USA
[3] Youngstown State University, Youngstown, OH
[4] Vassar College, Poughkeepsie, NY
[5] University of Toledo, Toledo, OH
[6] University of Manitoba, Winnipeg, MN, CANADA
[7] Department of Astronomy and Astrophysics, The Pennsylvania State University, University Park, PA 16802, USA
[8] NASA's Goddard Space Flight Center, Greenbelt, MD
[9] University of Virginia, Charlottesville, VA
[10] NRAO, Charlottesville, VA
[11] Instituto de Astronomia, Geofísica, e Ciências Atmosféricas da Universidade de São Paulo, São Paulo, Brazil
[12] STScI, Baltimore, MD

Local Hickson Compact Groups (HCGs; Hickson 1993) are therefore promising testbeds for investigating morphological galaxy transformations nearby that are directly relevant to galaxy evolution from 'blue cloud' to 'red sequence' in the color-absolute magnitude plane (e.g., Hogg et al. 2004; Balogh et al. 2004; Willmer et al. 2006). In dense environments at present, this change likely occurred at $z = 1$–2 (e.g., Cucciati et al. 2006; Franzetti et al. 2007; Cooper et al. 2007). Of the nearest HCGs, HCG 31 (NGC 1741) is perhaps the best example of catching this process in progress. This system is comprised entirely of low mass (1–8×10^9 $M_\odot$; Verdes-Montenegro et al. 2005), late-type galaxies in a compact ($\sim 1.4'$ [~ 23 kpc] diameter) configuration. It is clear from Figure 1 that each of galaxies in the group is disturbed, and tidal tails, bridges, and dwarfs are prominent.

In this paper, we present deep, three band *HST* ACS images of HCG 31, using high angular resolution and sensitivity to probe modes of star formation from the star cluster ($\sim$pc) to star complex and dwarf galaxy ($\sim$kpc) scale. Our goal is to investigate whether this system is a valid analogue of $z = 1$–2 galaxy evolution in the context of hierarchical structure formation in dense environments. In particular, we want to study the mechanism by which neutral gas is consumed in dense and dynamically young environments.

1.1. *Studies of HCG 31 to Date*

From visual inspection of Figure 1, the primary galaxies that comprise HCG 31 (A+C, B, and G) are clearly disturbed, and the presence of bright tidal structures (E, F, and H) further supports the importance of gravitational interactions in the recent history of the system. An additional galaxy, Q to the north, is shown to be part of the group based on radial velocity (Rubin et al. 1990) and H I structure (Verdes-Montenegro et al. 2005) that link it to other group members. UV, optical, and infrared photometry of A+C indicate active recent and ongoing star formation (e.g., Iglesias-Paramo & Vilchez 1997; Johnson et al. 1999; Johnson & Conti 2000; Johnson et al. 2007). This conclusion is supported by spectroscopic detections of Wolf-Rayet signatures in A+C and F (Kunth & Schild 1986; Rubin et al. 1990; Conti 1991; López-Sánchez et al. 2004).

The high levels of star formation and irregular morphology of the A+C complex imply a recent starburst triggered by their mutual interaction. Further study of the H I morphology and velocity field of the entire system indicates that not just one but multiple interactions have led to the current configuration (e.g., Amram et al. 2004; Mendes de Oliveira et al. 2006). Notably, much of the neutral hydrogen in the group has been removed from the galaxies (Verdes-Montenegro et al. 2001) yet remains bound to the group in tidal structures; 60% percent of the H I is located in four tidal tails and one bridge linking six of the member galaxies (Verdes-Montenegro et al. 2005). In sum, though the group as a whole is not H I deficient, the *individual galaxies* are (Verdes-Montenegro et al. 2001).

While Rubin et al. (1990) conjectured that HCG 31 will coalesce into a single large elliptical in only a few orbital periods, this is still an open issue. Specifically, will HCG 31 transition in the near term (within ~ 1 Gyr) into an evolved state such as a 'fossil group' – a single, elliptical galaxy with a bright X-ray halo (Jones et al. 2003)? As HCG 31 is one of the most compact groups in the Hickson et al. (1992) Atlas with most of the H I stripped from its individual galaxies, it is perhaps the most likely candidate for a late-stage merger (Williams et al. 1991).

Can the modes of star formation — from the populations of parsec-scale star clusters to kpc-scale star-forming complexes and dwarf galaxies — in this compact galaxy group elucidate the mechanism of galaxy transformation in the high redshift universe? With our new ACS imaging as well as spatially resolved IR constraints on the current star formation rates (SFRs) throughout the system, we aim to shed new light on the current state of star formation in HCG 31 as well as its future evolution.

At the H I redshift, $z = 0.01347 \pm 0.00002$ (Meyer et al. 2004), of HCG 31, its distance is 58.3 Mpc (yielding a distance modulus of $DM = 33.83$) and $1''$ corresponds to 275 pc ($\Omega_{\rm M} = 0.3$; $\Omega_\Lambda = 0.7$; $h_{100} = 0.7$; Spergel et al. 2007). Using a Galactic $E(B-V) = 0.051$ (Schlegel et al. 1998), all magnitudes and colors throughout the text have been corrected for Galactic reddening.

2. OBSERVATIONS

Observations of HCG 31 were obtained with *HST* ACS/WFC using the F435W, F606W, and F814W filters. Throughout, we use B_{435}, V_{606}, and I_{814} to refer to the F435W, F606W, and F814W ACS filters and the magnitudes measured in those filters, respectively. The data were taken on August 8, 2006 with exposure times of 1710 seconds in F435W, 1230 seconds in F606W, and 1065 seconds in F814W. The observations for each filter were taken with three equal exposures, using a three-point dither pattern. The implementation of `MultiDrizzle`[13] in the *HST*/ACS data pipeline provides combined, geometrically corrected, and cosmic ray cleaned images. For the analysis of point sources, we used the standard *HST* pipeline products with a nominal pixel scale of $0\farcs05$ per pixel. For analysis of the extended sources, we ran `MultiDrizzle` with the pixel scale set to $0\farcs03$ per pixel to improve the spatial resolution.

In addition to the new *HST* observations that are the primary focus of this paper, we also present new *Swift* and *GALEX* observations of HCG 31, as well as incorporate the *Spitzer* IRAC and MIPS images presented in Johnson et al. (2007). This is part of a long-term, indepth multiwavelength investigation into a sample of 12 HCGs using the combination of *HST* three-color imaging (six complete), *Chandra* ACIS imaging spectroscopy (eight total as part of archival and new observations), *Spitzer* IRAC and MIPS imaging (already in hand; Johnson et al. 2007), and *Swift* Ultraviolet Optical Telescope (UVOT) and *GALEX* multifilter imaging (Tsanavaris et al., in prep.).

For the purposes of associating star-forming structures within the individual features in HCG 31, we have defined polygonal boundaries for the galaxies and tidal regions as marked on the ACS V_{606} image shown in Figure 2.

[13] `MultiDrizzle` is a product of the Space Telescope Science Institute, which is operated by AURA for NASA. See http://stsdas.stsci.edu/pydrizzle/multidrizzle.

2.1. *Star Cluster (SC) Candidate Identification and Photometry*

At the redshift distance of HCG 31 of 58.3 Mpc, star clusters are expected to be unresolved or marginally resolved with a 0.″05 ACS pixel corresponding to 13.8 pc. Therefore, as a first step to finding star cluster candidates, the entire ACS field was searched for point sources.

Point-source photometry was performed on the pipeline-drizzled images using the point source function (PSF) fitting algorithm of Stetson (1987) as implemented in IRAF.[14] Given that the V_{606} image was the deepest of the three, it was the primary one used for point-source identification and filtering. Magnitudes are given in the Vega system using the zeropoints appropriate for August 2006:[15] 26.406, 25.767, and 25.520, for V_{606}, B_{435}, and I_{814}, respectively.

We searched for point-source candidates using the median-divided V_{606} image with a threshold of 0.25σ. The weight-map image from the pipeline processing was used to filter the candidate list to remove artifacts from chip edges and the diffraction spikes from saturated stars; point source candidates were rejected if their weight map values were less than the median minus twice the standard deviation of the distribution. Visual inspection confirmed that this method effectively screened out spurious detections without discarding real point sources.

PSF models in each filter were constructed from the brightest, isolated, and unsaturated stars. Their radial profiles were checked for irregularities, and 13, 13, and 18 PSF stars were used in V_{606}, B_{435}, and I_{814}, respectively. Moffat functions were used to fit the PSF in each case, with a constant PSF in V_{606}, and linearly variable PSFs for B_{435} and I_{814}. The `daophot` photometry was compared to aperture photometry for the PSF stars within a 0.″5 (10 pix)-radius circular aperture in order to determine the aperture correction. To these values, the aperture correction from 0.″5 to infinity from Sirianni et al. (2005) was added. Finally, the photometry was corrected for Galactic extinctions of A_{606}=0.144, A_{435}=0.210, and A_{814}=0.093.

For the final star cluster (SC) candidate catalog, objects were required to be detected in all three filters with magnitude error $\sigma_{\rm mag} < 0.3$ and $-2<$ *sharp* <2 (*sharp* is a measure of the width of the data relative to the model psf; *sharp* = 0 indicates a width well-matched to the psf) in each and $\chi < 3$ in I_{814}. We used I_{814} for the χ criterion because the model PSF is best determined in that image. Furthermore, if SC candidates are marginally resolved because of nebular Hα emission, this will not be a factor in I_{814}. (We do not want to eliminate these interesting candidates from our catalog.) Finally, color cuts of B_{435}–V_{606}< 1.5 and V_{606}–I_{814}< 1.0 were imposed to reduce contamination from foreground Galactic stars. These cuts were chosen based on distinct clumps of sources in color-color space. The SC candidate numbers by region are given in Table 1. To identify the youngest clusters with nebular emission, we draw a diagonal line in Figure ?? that crosses the evolutionary tracks with nebular emission at $\tau \sim 5 \times 10^6$ yr. This conservative line takes into account typical photometric errors such that all SC candidates to the left of that line have colors significantly distinct from the evolutionary tracks without nebular emission. The fraction of SC candidates in this region of color-space is indicated in column 4 of Table 1.

We imposed stricter point-source selection criteria to identify globular cluster candidates. Following Rejkuba et al. (2005), we used a hyperbolic filter in the sharpness vs. magnitude plane and a hyperbolic filter in the magnitude error vs. magnitude plane set using the output photometry from the V_{606}-band completeness tests (see §2.2) to include $\sim$ 97% of the detected artificial point sources. Point sources were also required to have $\sigma_{\rm mag} \leq 0.3$, $\chi \leq 3$, and $-2 \leq$ *sharp* ≤ 2 in all three filters. These criteria rejected a large fraction of the brightest ($M_{\rm V_{606}}< -9$) and bluest (in V_{606}–I_{814}) point sources, indicating that many of them are marginally resolved. This is perhaps not surprising, as the wide V_{606} filter includes Hα emission, and most of these sources have colors consistent with a strong nebular contribution. The spatial scale of the Hα-emitting region surrounding a young star cluster is frequently larger than that of the stars alone. Those candidates with colors consistent with older star clusters are typically fainter and unresolved, as expected.

2.2. *Completeness*

Using `addstar` in the `daophot` package, we added 3000 artificial stars to the pipeline-drizzled V_{606} image evenly distributed between magnitudes 24 through 28 (before aperture and extinction corrections), and then ran the photometric pipeline on these data. Sources were considered detected if their input and output positions matched within 0.″075 (1.5 pix). Using the distributions of sharpness, *sharp*, vs. magnitude, and magnitude error, $\sigma_{\rm mag}$, vs. magnitude, we set hyperbolic filters following the procedure of Rejkuba et al. (2005) to classify point sources. All point sources were also required to have $\sigma_{\rm mag} \leq 0.3$, $\chi \leq 3$, and $-2 \leq$ *sharp* ≤ 2. Of the detected sources, these filters eliminated an additional $\sim$ 3%. From the ratio of numbers of detected point sources to input artificial stars as a function of magnitude, the V_{606} 90% and 50% complete magnitude limits were found to be 26.43 and 27.42 (including aperture and extinction corrections), respectively. For the B_{435} and I_{814} tests, the same input artificial star catalog was used as for the V_{606} image with the positions corrected for the image offsets. The V_{606} detected objects were then run through the B_{435} and I_{814} photometric pipelines. Objects were filtered using only the constant absolute $\sigma_{\rm mag}$, χ, and *sharp* limits defined above, which eliminated $1-2$% of the sources. The subsequent B_{435}/I_{814} 90% and 50% completeness limits were 26.73/26.51 and 27.33/27.18, respectively. Given the different aperture and extinction corrections in each filter, the input artificial star catalog had effective colors of B_{435}–V_{606}= -0.13 and V_{606}–I_{814}= 0.04.

Given that most of the young SC candidates are located within the group galaxies, we also determined the completeness limits within A+C and B, with boundaries corresponding to the regions shown in Figure 2 where the average surface brightness and background noise are considerably higher. The 90% $V_{606}/B_{435}/I_{814}$ complete-

[14] IRAF is distributed by the National Optical Astronomy Observatory, which is operated by the Association of Universities for Research in Astronomy (AURA) under cooperative agreement with the National Science Foundation.

[15] http://www.stsci.edu/hst/acs/analysis/zeropoints/

ness limits are 25.02/24.96/25.10. For a distance modulus of 33.83, these limits are fainter than the apparent magnitude of 24.83 corresponding to an absolute V_{606} luminosity limit of $M_{\mathrm{V}_{606}} < -9$.

2.3. *Star-Forming Complexes*

Complexes in HCG 31 were identified from the B_{435} and composite images, visually and with the use of contour plotting, and measured from the custom multidrizzled images (1 pix = 0.″03). They were typically larger than ∼20 pixels in diameter (corresponding to ∼150 pc), with outer boundaries ∼10σ above the background. There were 40 such complexes: 11 each in regions A+C, B, and G, 3 in region E, and 4 in region F, as shown in Figure 11 and listed in Table 2. The complexes in Region G correspond to the “optical knots” noted in ground-based unsharp-masked B-band images by Verdes-Montenegro et al. (2005). A visual examination of ground-based g and i images (Mendes de Oliveira et al. 2006) found no complexes of comparable size or brightness in the northern galaxies Q and R outside of the ACS field of view.

The complex diameters in HCG 31 range from ∼150 to 875 pc. In nearby spirals, the sizes of the largest complexes scale with the absolute magnitude of the galaxy (Elmegreen et al. 1994, 1996) and range from ∼150 pc for M_B=–16 to ∼1500 pc for M_B = –21. The absolute V magnitude for HCG 31 A+C is –20.7 (for DM = 33.83; Conti 1991), with M_B = –20.0 based on our *HST* image; its complex diameters range from 190–540 pc. B and G are measured to have M_B of –18.5 and –18.9, with complexes ranging from 165–190 pc and 140–400 pc, respectively. These are comparable to the sizes of complexes in local spirals with similar absolute magnitudes. The complexes in the tidal debris of HCG 31 are anomalously large; region E, with M_B= –16.5, has a complex with a diameter of 875 pc, and region F, with M_B= –15.8, has a complex of 550 pc. These values are comparable to what is observed in local Blue Compact Dwarf (BCD) galaxies and factors of 2–3× larger than those in Sm and irregular galaxies of similar magnitudes (Elmegreen et al. 2006).

2.4. *Evolutionary Track Models*

We used the evolutionary tracks of the Bruzual & Charlot (2003) instantaneous burst model assuming a Salpeter initial mass function (IMF), a stellar mass range from 0.1–100 M$_\odot$, and 1/5 solar metallicity, consistent with the range of $Z/Z_\odot$=0.2–0.4 found by López-Sánchez et al. (2004) for this system. The spectra at each grid point in time have been convolved with our filter set to obtain colors and magnitudes.

The Bruzual & Charlot (2003) models do not include a contribution from nebular emission. Emission lines such as Hα and [O III] can significantly affect the colors of star clusters with ages ≤ 10 Myr. Given that the F606W filter is quite broad, strong Hα emission at the redshift of HCG 31 will boost the V_{606} fluxes, thereby reddening the B_{435}–V_{606} colors and making the V_{606}–I_{814} colors bluer (e.g., Vacca & Conti 1992; Conti et al. 1996). To calculate evolutionary tracks that incorporate a model of nebular emission, we used the `Starburst99`[16] (Leitherer et al. 1999) emission-line strengths for Hα and Hβ for the same IMF and metallicity burst as given above. Another strong line is [O III], which is not included in the `Starburst99` models. To estimate the maximum contribution of [O III] to the colors, we used the most extreme value of 0.7 for the ratio of log([O III]/Hβ) observed in the KISS sample of low-mass star-forming galaxies (e.g., Salzer et al. 2005) to estimate [O III] luminosity as a function of time.

[16] http://www.stsci.edu/science/starburst99/

2.5. *Intrinsic Reddening*

The colors of young star clusters are often reddened by the dusty clouds in which they are born. The magnitude and direction of an A_{606}=1 Galactic reddening vector (Cardelli et al. 1989) is plotted in the color-color and color-magnitude diagrams (see Fig. 5). This may not be appropriate for these galaxies, given their lower metallicities ($Z/Z_\odot$ = 0.2–0.4; López-Sánchez et al. 2004), but is conservative and consistent with convention in the literature. The V_{606} filter covers strong nebular emission lines such as [O III] and Hα from the youngest star clusters at the redshift of HCG 31, and as we showed in §2.4 the inclusion of this flux moves the predicted evolutionary tracks to the bottom left portion of the left-hand panel in Figure 5, nicely localizing very young star clusters still surrounded by interstellar material in color-color space. The reddening vector is nearly perpendicular to the tracks including nebular emission. Therefore, as long as extinction does not push too many star clusters below our selection criterion, the youngest clusters will still be identified as such.[17] This is not the case however, for older clusters which no longer ionize nearby interstellar gas. In this situation, shown as the solid line in the same Figure, the reddening vector is nearly parallel to the tracks themselves, making it difficult to quantitatively estimate the total extinction on a cluster by cluster basis. The colors therefore give upper limits for age estimates.

We can get an independent assessment of extinction on larger physical scales from mid-infrared observations taken with the IRAC instrument on *Spitzer*. From the *Spitzer* IRAC images presented in Johnson et al. (2007), the strongest dust emission is present at the A+C interface. This is illustrated in the ‘non-stellar’ IRAC image shown in Figure 3. This image is composed of the 4.5μm image divided by the scaled 3.6μm image to emphasize emission in excess of that expected from the Raleigh-Jeans tail from stars. Galaxy B is quite faint, and the tidal debris is largely invisible; therefore we do not expect significant dust extinction on average in those regions. The assymmetry in the disk of G is more prominent in this representation. Therefore, in general we expect dust extinction will be most problematic in A+C and the western star-forming ring of G.

2.6. Swift *and* GALEX *UV Imaging*

We used UV observations taken with *Swift*/UVOT and *GALEX* to probe star formation activity in HCG 31 (see Tzanavaris et al., in preparation for details). Briefly, we calculated background-subtracted fluxes at the effective wavelengths of the U, $UVW1$, $UVM2$, $UVW2$

[17] An assumption underlying this assertion is that ionizing stellar flux must be able to escape its natal dust cloud and still encounter sufficient gas to create detectable nebular emission.

UVOT filters (3501, 2634, 2231, 2030Å) and the FUV and NUV *GALEX* filters (1528 and 2271Å) in the galaxies and tidal structures for which Johnson et al. (2007) performed IR photometry. Currently, star formation estimates are complicated by dust attenuation concerns, and we present initial results here for which we have only corrected for Galactic extinction (Schlegel et al. 1998; Cardelli et al. 1989). No corrections for intrinsic extinction are included. Even so, the conversion of UV flux to star formation rate from Kennicutt (1998) indicates strong star-formation activity in this group in agreement with estimates in other wavebands (see §3.3). In particular the significant flux levels in the *Swift* $UVW2$ and *GALEX* FUV filters are indicative of stellar populations characterized by massive stars with ages of a few Myr. This is consistent with previous UV work that only covered a small area in the central region of A+C (Conti et al. 1996). The *GALEX* NUV data has been included as purple in Figure 1, and is consistent with the *Swift* $UVW2$ emission.

2.7. *Multicolor Images*

Given the wealth of information from the optical, infrared and ultraviolet images, we have constructed two multicolor images. The first incorporates images from five bands: *GALEX* (NUV), *HST* (B_{435}, V_{606}, and I_{814}) and *Spitzer* (8 μm), and the second is a three-color composite of *HST* data only. All data were converted to flux density units of erg s^{-1} cm^{-2} Å^{-1}. These values were initially distributed to the greyscale range logarithmically. The `Karma` visualization package (Gooch 1996) was used to rotate the data and regrid the non-*HST* data to the *HST* pixel scale. It was also used to further adjust the greyscales, for example, to emphasize the brightest regions in the non-*HST* data. The remaining data manipulation was done using `GIMP`.[18] Following the methods in Rector et al. (2007), color was assigned (B_{435} = blue, V_{606} = yellowish green, I_{814} = red, NUV = purple, and 8 μm = orange) and the images combined using the screen algorithm. Masks were applied to remove the ghost reflection and to reduce the UV emission from the foreground star. Selected regions of the tail were brightened, because ensuring the a dark background decreases the brightness of faint astronomical objects.

3. RESULTS AND DISCUSSION

3.1. *SC Candidate Luminosity Functions*

The luminosity function of star clusters can be approximated by a power law, $dN/dL \propto L^{\alpha}$, with $\alpha \approx -2$, in many spirals, starbursts, and merging galaxies (see compilation in Whitmore 2003 and references therein). This strong similarity in the cluster populations across galaxies types and with very different star formation rates led Whitmore (2003) to suggest that the basic properties such as age, mass, and luminosity, of star cluster systems in nearby, actively star-forming galaxies could be broadly understood from simple statistics. In general, the luminosity of the brightest young cluster (Larsen 2002; Whitmore 2003) in a galaxy scales with the total number of clusters in the system brighter than $M_{\mathrm{V}_{606}} = -9$, regardless of whether the galaxy is quiescent or starbursting, dwarf or giant, interacting or isolated. Given a universal power-law luminosity function for young star clusters, galaxies with high star formation rates, and therefore larger star cluster populations, are more likely to populate the luminous end of the luminosity function.

In Figure 4, we construct the V_{606} luminosity function for individual galaxies in HCG 31, a dynamical environment with on-going, multiple interactions that is different than those studied previously. The power-law index α is calculated from the best-fit index β in these distributions as: $\alpha = 2.5 \times \beta + 1$, and lies between ≈ -1.8 and -2.3 for each galaxy. To improve statistics, we also summed clusters from all galaxies together to obtain an index $\alpha \approx -2.1$. This is well within the range found for cluster systems in very different galaxies. We show the relationship between the brightest cluster and the total number of clusters brighter than $M_V = -9$ for each galaxy in Figure 8. The line in this figure shows that the best fit relation determined by Whitmore et al. (2007) from 40 galaxies (not including any in compact groups) nicely describes the location of the HCG 31 galaxies in this parameter space. The scatter in HCG 31 is also well within that observed.

These results suggest that despite the unusual environment of a compact group, there are no obvious differences in the distribution of star cluster luminosities and numbers when compared with more typical environments locally.

3.2. *Ages and Spatial Distributions of Star Cluster Candidates*

The age distribution of star clusters provides important information on their formation and disruption, and can be determined by comparing the integrated cluster colors with the predictions of stellar population models. Star cluster candidates have been sorted according to the structures within HCG 31 they are spatially associated with as drawn in Figure 2. From inspection, the majority of the SC candidates are spatially coincident with galaxies and tidal features in HCG 31, with only 4.4% (19 of 424) outside of these boundaries. Furthermore, the SC candidates positions within the color-color plot (Fig. 5) are generally consistent with instantaneous burst evolutionary tracks. Notably, a large fraction of the brightest clusters in each region are in the lower left section of Figure 5 as expected for the youngest clusters ($\tau \leq 10^7$ yr) and typical of galaxies currently forming stars. The few cluster candidates which fall up and to the left of the region where the nebular emission tracks connect to the rest of the models in the lefthand panel of Figure 5 are likely to be young blue clusters with little nebular emission. Though galaxy A+C is clearly where the largest fraction of young clusters are found, galaxies B and G also have significant populations of young clusters with colors consistent with nebular emission.

Many of the cluster candidates in the HCG 31 galaxies fall in a clump in color-color space around V_{606}–$I_{814} \approx 0.4$ and B_{435}–$V_{606} \approx 0.2$, near the region where the tracks which include nebular emission join those which do not, forming an almost continuous sequence. Young clusters often have at least modest amounts of extinction associated with them or their parent galaxies, but we are

[18] Gnu Image Manipulation Package (GIMP) written by Peter Mattis and Spencer Kimball and released under the GNU General Public License.

unable to correct for this extinction on a cluster by cluster basis because reddening due to dust is degenerate with age in the filter combination used here. Therefore, we can place only an upper limit on the age of any given cluster. Regardless of this limitation, the color-color diagrams reveal interesting features.

Our cluster sample consists of all objects brighter than an $M_{\mathrm{V}_{606}}$ of -9, where we have only corrected for foreground extinction. Whitmore et al. (1999) have shown that selecting only objects with $M_V \leq -9$ returns a very clean sample of star clusters, because this limit is brighter than all but the most luminous stars. The critical observation is that the number of clusters brighter than $M_V \leq -9$ in each galaxy drops rapidly at redder colors (older ages) along the tracks. Because clusters fade rapidly with age, a number of them will naturally fade below a given magnitude or luminosity and be lost from the sample. Therefore, this sample is not sensitive to lower mass clusters at older ages (though see §3.4 for a discussion of globular cluster candidates), which can partially explain the lack of many clusters with redder colors.

We can interpret the color (or equivalently, a crude age) distribution of clusters in Figure 5 by considering the results from simple statistical cluster population models (e.g., Whitmore et al. 2007). Specifically, the formation and evolution of star cluster systems can be approximated statistically by following simple formulae, because star cluster systems in galaxies of different types show regularities, such as a very similar power-law luminosity function as discussed above. Chandar, Whitmore, & Fall (in preparation) predict the number of clusters expected for a simple model which assumes that clusters form at a constant rate with an initial power-law mass function, $dN/dM \propto M^{-2}$, where none of the clusters are destroyed. For this simple model, assuming a single V_{606} luminosity limit to mimic our selection procedure, the number of clusters increases each decade in age, by factors of ≈ 2 ($10^7 - 10^8$ yr) and ≈ 4 ($10^8 - 10^9$ yr) over the number of $10^6 - 10^7$ yr clusters. The distribution of cluster colors in HCG 31 galaxies however, shows that the opposite trend is observed, with the number of clusters falling off rapidly with color (age) for HCG 31 galaxies redward of the clump of clusters mentioned above at ages $\approx$few$\times 10^7$ yr.

This rapid decline in the number of clusters with redder colors, observed for all of the galaxies, is due to the formation or disruption of the star clusters, or to some combination of both. A rapid decline in the number of clusters observed with age (or color) has been observed previously in several galaxies, including the Antennae (e.g., Fall et al. 2005; Whitmore et al. 2005), the solar neighborhood (Lada & Lada 2003), and the Small Magellanic Clouds (Chandar et al. 2006). The early, rapid disruption of clusters at ages $\tau \lesssim 10^8$ yr is plausibly dominated by two physical processes internal to the clusters themselves: the disruption of star clusters by the expulsion of interstellar material left over from star formation, and mass-loss from continued stellar evolution (Fall, Chandar, & Whitmore, submitted). Because these internal processes are largely independent of environment, they should disrupt clusters in a similar way in most galaxies. This picture predicts that the number of clusters in a luminosity-limited sample should decline with age (or towards redder colors), very similar to the pattern observed here for several galaxies in HCG 31, even with a constant star formation rate. Therefore, despite the seemingly unusual environment of a compact group, there are no obvious differences in the distribution of star cluster luminosities and numbers when compared with more typical environments.

An alternative explanation is that all of these galaxies in HCG 31 have experienced a very large, recent, coordinated burst of cluster formation. These galaxies have a range of star formation rates, (see §3.3), indicating that some galaxies are interacting more strongly than others. For example, the most actively star-forming galaxies are A and C, which are interacting directly with one another. Though this interacting/merging galaxy pair is forming stars at a higher rate than galaxy G, and these galaxies do not resemble each other morphologically at all, the general distribution of their colors/ages are quite similar. In a typical environment, there is no reasonable physical mechanism for coordinating star formation on such large scales given a characteristic speed of bulk motions in the ISM of $\sim 100\,\mathrm{km\,s^{-1}}$. However, in HCG 31, A+C, G, and B as well as the tidal features E, F, and H, are connected by a common H I envelope of tails and bridges, and each region is undergoing a significant rate of star formation given their galaxy types (see §3.3). Therefore, while the SC candidate distributions of colors and luminosities are likely to be significantly shaped by the mechanisms of creation and disruption common to all star-forming galaxies, it is clearly the case that star formation in this group as a whole has been recently elevated as a result of the multiple interactions.

3.3. *Star Formation Rates*

A galaxy's 24 μm luminosity has been shown to be a good tracer of star-formation activity, especially for galaxies without a strong contribution from old stellar populations. To the *Spitzer* 24 μm photometry for the HCG 31 galaxies published in Johnson et al. (2007), we applied the calibration of Calzetti et al. (2007) to obtain star-formation rate (SFR) estimates which are listed in Table **??**. The total SFR for all galaxies is ~ 3.8 $\mathrm{M}_\odot$ yr^{-1}, with the largest contribution ($> 80\%$) due to the combined emission from A+C and E (unresolved in the 24 μm *Spitzer* images). This is in good agreement with previous estimates using different SFR indicators, such as Hα, far-IR, 60μm and 1.4 GHz, which give estimates ranging from 2–8 $M_\odot$ yr^{-1} (Dopita et al. 2002; Richer et al. 2003; López-Sánchez et al. 2004; López-Sánchez & Esteban 2007) for the whole group.

As an independent means of constraining the SFR with the new *HST* data, we examined the SC candidates with colors consistent with $\lesssim 5$ Myr star clusters with nebular emission (see §2.1 and the lefthand panel of Fig. 5). Summing the masses of these clusters and dividing by the integrated time on the nebular evolutionary track will give an estimate of the average cluster SFR over this epoch. To convert the colors to an age, the B_{435}–V_{606} vs. V_{606}–I_{814} axes were rotated so that the reddening vector was vertical. For most of the track, the horizontal position in this rotated color space increases monotonically with time. The colors of the SC candidates designated as having nebular colors were then projected onto the appropriate evolutionary track, and the distance to the track was recorded as the intrinsic reddening of the cluster. (Negative distances were set to 0.) This gave a mean extinction value for the sample of $A_{606} = 0.74$. The V_{606} magnitude of each SC candidate was then corrected for its intrinsic reddening and converted to a mass. Following this algorithm, we obtained a cluster SFR of ~ 1 M$_\odot$ yr^{-1}, within a factor of a few of the estimate from the completely independent 24μm emission. If interpreted literally, this suggests that approximately one-quarter of newly formed stars are still associated with their natal star clusters at these early times. Caveats to this statement include the unknown systematic uncertainties in translating color and magnitude to age and mass as well as the unquantified incompleteness to low mass and very highly extincted clusters.

3.4. *Globular Clusters in HCG 31*

Some of the point sources from Figure 5 are expected to be old ($\tau > 10$ Gyr) globular clusters (GCs) in the HCG 31 system. Though GCs have been studied in only a few HCGs to date (Barkhouse et al. 2001; Da Rocha et al. 2002b), they can be used to provide information on the formation and early evolution of such systems (e.g., Brodie & Strader 2006).

Use of color-color diagrams to identify such clusters has proven very effective (e.g., Rhode & Zepf 2001, 2004). The color-color diagram for all point sources with V_{606}< 26 (where we expect over 50% completeness for old clusters) in the entire HCG 31 field is plotted in Figure 9. To define the color range for globular clusters in the ACS VEGAmag system, we have used the reddening corrected $B-V$ and $V-I$ colors for 97 Milky Way globular clusters (those with BVI magnitudes) from the Harris (1996) catalog. The color range $0.55 < (B-V)_0 < 1.05$ and a 0.2 mag wide swath in $(V-I)_0$ centered on the relation $(V-I)_0 = 0.82(B-V)_0+0.36$ was found to contain 94% of the clusters. This GC bounding region was then transformed to the ACS VEGAmag system (Sirianni et al. 2005), and is shown in Figure 9.

A total of 43 point sources with V_{606}< 26. (for $M_{\rm V_{606}}< -7.8$ at the distance of HCG 31) have error ellipses that overlap the bounding region, and are thus considered candidate globular clusters in HCG 31. The vast majority of these objects are centered on the primary galaxies in the group. Although some background elliptical galaxies and foreground Milky Way dwarf stars with similar colors are expected to contaminate our sample, the paucity of such objects over most of the field (coded as 'Other' in Figure 9) shows that the vast majority of objects are likely true GCs in HCG 31. We have used the Besançon Milky Way stellar population model (Robin et al. 2003) to estimate the number of foreground Milky Way stars with magnitudes and colors consistent with our GC selection region; we expect a total of 2 to 3 objects over the entire ACS field for the stellar density of 0.23 objects arcmin^{-2}, consistent with the number of objects (2) that already clearly lie outside the defined HCG 31 regions. Therefore, background contamination is not significant in our candidate GC sample. Inspection of the color-color plot of strictly defined point sources supports our conclusion that the vast majority of objects with nebular colors are marginally resolved; only two point sources with nebular colors (as defined in Figure 5) and $M_{\rm V_{606}}< -9$ satisfy the point source selection criteria.

Studies of GCs in late-type galaxies such as these are made extremely difficult by the rapidly varying background close to the centers of the galaxies, and there is a real possibility that some objects suffer additional internal extinction. As a result, some of our GC candidates may well be younger objects that have been significantly reddened (note the reddening vector in Figure 9). Furthermore, the detection of objects close to the galaxy centers may be adversely affected by photometric incompleteness – the 90% completeness level for point sources within the HCG 31 subsections (see §2.2) are significantly brighter than outside the galaxies.

From inspection of the color-magnitude diagrams for the GC candidates, we find that while many of the candidates are spatially close to their parent galaxies, the large number close to the average 90% completeness limits rather than the brighter galaxy core limits, indicates that the former are more appropriate. As a result, we have adopted a fraction $f = 0.9 \pm 0.1$ for all objects with V_{606}< 26. This is certainly not applicable for a small number of objects very close to the galaxy centers, but these will not affect the basic results from our study.

A further test on the effects of incompleteness can be gleaned from the V_{606} luminosity function of the candidates, shown in Figure 10. While the number of GC candidates is small, the luminosity function does show the general property expected for a globular cluster system: a monotonic rise towards the turnover of the GCLF. Also plotted is the expected GC luminosity function assuming a peak at $M_V \sim -7.4$ ($V_{606} = 26.3$ for $(m-M) = 33.83$, $V-I = 1.0\pm0.3$), and a dispersion $\sigma = 1.2$ (Harris 2001). That the data continue to rise very sharply to V_{606}= 26 again suggests that photometric incompleteness due to varying galactic backgrounds are not strongly affecting our numbers.

From the expected GC luminosity function (as plotted in Figure 10), we estimate that the GCs brighter than V_{606}= 26 are 40 ± 7% of the total GC distribution, where the errors reflect added uncertainties of 0.2 mag in the GC luminosity function dispersion, and an uncertainty of 0.2 mag in the location of the peak magnitude. To estimate the total number of GCs in each galaxy in HCG 31, we first correct our observed numbers N_{obs} (and associated Poisson errors) by our bulk completeness fraction $f = 0.9 \pm 0.1$, and then correct for the fraction of the luminosity function we can observe. The final, corrected total number of GC candidates are given in Table 1, where we have also included the single GC candidates superposed on the tidal features E and F. We have made no corrections for the (small) background contamination derived above. Fortunately, both the large distance to HCG 31 and the compactness of the GC systems in these low-mass galaxies mean we are essentially observing the *entire* GC system, and so we make no corrections for any clusters outside the ACS field of view.

Column 6 of Table 1 shows the specific frequency S_N, or the number of GCs normalized to the V-band luminosity $M_V = -15$ (Harris & van den Bergh 1981).[19] The

[19] While the number of GCs per unit mass (the T parameter from Zepf & Ashman (1993)) is now commonly used to compare numbers of clusters between differing galaxy types, all galaxies in

values of S_N for each of the larger galaxies A+C, B and G are all consistent with the lower values expected for late-type galaxies in other environments ($S_N \sim 0.5-0.9$; e.g. Goudfrooij et al. 2003; Chandar et al. 2004; Rhode et al. 2007). From this, there is no evidence that these galaxies have undergone previous mergers that formed a significant population of new massive star cluster populations.

3.5. *Intragroup Stellar Populations?*

The lack of a significant number of GC candidates far outside the galaxies may also indicate a dynamically young system, because galaxy interactions are expected to liberate some stars (and star clusters) from the gravitational potentials of their parent galaxies. Indeed, some compact groups do show significant amounts of diffuse light (e.g., Pildis et al. 1995; White et al. 2003; Da Rocha & Mendes de Oliveira 2005; Da Rocha et al. 2008). Does a significant diffuse component (in the form of intergalactic GCs) exist in HCG 31? As there are only two objects that lie significantly outside the small globular cluster systems concentrated in the primary galaxies (broadly consistent with the expected number of foreground Milky Way stars), there is no significant population of intragroup GCs present in our field. However, we can put a meaningful upper limit on the presence of such a population.

To quantify this further, we first assume that both GC candidates outside the galaxies are indeed intragroup systems. We define the fraction of intergalactic cluster light as $f_{IC} = L_{IC}/(L_{gal} + L_{IC})$, where L_{gal} is the combined V-band luminosity of the HCG 31 galaxies and L_{IC} is the total luminosity of the intergalactic population. Using the $M_{\rm V}$ value of Conti (1991) converted to our value of the DM, we find a combined $M_{V,group} = -20.7$, or $L_V \sim 15.5 \times 10^9$ $L_{\odot,V}$. Given the two intergalactic GC candidates located far from the HCG galaxies, and subtracting the expected contamination of two stellar objects, we have an observed $N_{IGC,obs} = 0 \pm 2$, or (correcting for the missing part of the luminosity function) an upper limit of 6 intergalactic GC candidates in the ACS field. Adopting a mean group specific frequency $S_N = 0.6 \pm 0.3$ (appropriate for the late type galaxies in HCG 31), this upper limit corresponds to a V-band luminosity of $\sim 0.9 \times 10^9 L_{\odot,V}$. Thus we place an upper limit of 5% on the intergalactic light in HCG 31. This low value of the intergalactic light fraction, when combined with previous work (where intragroup light fractions in other HCGs can be as high as almost 50%) is suggestive that the range of galactic properties, physical conditions, and dynamical history in the compact group environment may be extremely important in understanding the different processes that shape group evolution.

While our estimate above suggests there is very little (if any) intragroup light in HCG 31, a caveat here is that all galaxies in the group are rather low mass, with compact GC systems concentrated over a small ($r < 10$ kpc) radial extent (Rhode et al. 2007), so while it is possible that the interaction history of HCG 31 is so recent as to not have liberated much of an intergalactic population (consistent with the other observations presented here), it is unclear whether many GCs would be readily removed from such spatially concentrated GC systems in any case.

3.6. *Large Scale Star Formation*

Star-forming complexes represent the largest units of star formation in a galaxy (see review by Efremov 1995); they are typically kpc-scale regions encompassing several clusters. In local spirals, their masses and sizes approximately follow a power law distribution, and the largest ones scale with the host galaxy's absolute magnitude (Elmegreen et al. 1994, 1996). Complexes form from large-scale gravitational instabilities that depend on the local velocity dispersion, whether the region forms in a disk or a tidal stream. In disk galaxies, the Jeans length is about equal to the disk thickness, and complexes often appear as rather regularly spaced beads of star formation in normal spirals. Because a galaxy's largest complexes can be resolved even in high redshift galaxies, they are useful probes for comparisons of large-scale star formation in a variety of environments. In order to eliminate possible size-of-sample effects (discussed by Selman & Melnick 2000 but disputed by Vicari et al. 2002 and Elmegreen et al. 1994), complexes should be compared among galaxies with comparable absolute magnitudes.

Figure 7 shows a color-magnitude diagram including the HCG 31 complexes, coded according to their regions. Superposed are the evolutionary tracks discussed in Section §2.4. The complexes in region F are too blue for the basic tracks, and require the models that include nebular emission. We have used these tracks for all of the complexes, because a comparison with the Hα image of HCG 31 (Johnson & Conti 2000) shows that all of the complexes are associated with emission. Many of the complexes lie within the Hα knots identified from ground-based images by Iglesias-Paramo & Vilchez (1997). The complex masses range from $\sim 5 \times 10^5$ to $2 \times 10^7 M_\odot$; overall, the complexes average about $10^6 M_\odot$. The most massive ones are in E and in A+C; two of them in the central regions of A+C probably encompass more than one complex blended along the line-of-sight. The complexes are young, as expected by their Hα emission, with log(ages) ranging from about 6.5 to 7.5 years. The oldest ones are in regions A+C and B, in the central parts of those galaxies, which may also be due partly to blending with an older background.

The luminosities, L, of individual complexes scale approximately with their diameters, D, as $L \propto D^{1.8}$. This is essentially the same relation as that found for complexes in nearby quiescent spirals (Elmegreen et al. 2006; Elmegreen & Salzer 1999) and also in the gently interacting galaxy pair IC2163/NGC2207 (Elmegreen et al. 2001) at a distance of 35 Mpc. However, the absolute magnitudes of the complexes are $\sim$2 mag brighter in HCG 31 than in IC 2163/NGC 2207 (even though those galaxies are 1 and 2 magnitudes brighter than HCG 31 A+C, respectively) and in quiescent spirals with comparable or brighter total absolute magnitudes. The masses of the complexes in HCG 31 therefore are also higher, by a factor of $\sim$5–10. This suggests that the velocity dispersions may be higher in HCG 31 than in IC 2163/NGC 2207. The complex masses in HCG 31 resemble those in blue compact dwarf galaxies, which are also larger than those in normal spiral galaxies with the same absolute magnitudes. This result was inferred to be a consequence of

HCG 31 are late-type galaxies and the S_N values can be compared directly.

higher disk turbulence in blue compact dwarf galaxies (Elmegreen et al. 1996).

Hα Fabry-Perot observations by Amram et al. (2007) show velocity dispersions of typically 15–20 $\mathrm{km\,s^{-1}}$ over most of the regions in HCG 31, with values up to 30 $\mathrm{km\,s^{-1}}$ in the vicinity of the complexes. Elevated values in the immediate vicinity of the complexes probably result from extra turbulence generated by associated energetic events such as stellar winds and supernovae. Maps by Richer et al. (2003) with lower spatial and spectral resolution show velocity dispersions of 45 to 95 $\mathrm{km\,s^{-1}}$ over the main disk of galaxies A+C, with fairly constant values of $\sim$50 $\mathrm{km\,s^{-1}}$ in regions B, E, and F, and slightly higher values in region G. Although Hα velocity dispersions do not necessarily reflect the kinematics of the neutral gas out of which the complexes formed, the observed high large-scale Hα velocity dispersions in HCG 31 suggest that the disks and the tidal debris are more turbulent than the 5–10 $\mathrm{km\,s^{-1}}$ typical of quiescent spiral galaxy disks, which is consistent with the presence of more massive complexes.

Star formation is commonly observed in tidal features of interacting galaxies (e.g., Schweizer 1978; Mirabel et al. 1992). Numerical simulations indicate that complexes in such systems can form from interaction-triggered gravitational instabilities in the gaseous component (e.g., Elmegreen et al. 1993; Wetzstein et al. 2007). Complexes observed in tidal tails in the local interacting systems NGC 4485/90 (Elmegreen et al. 1998), the Leo Triplet galaxy NGC 3628 (Chromey et al. 1998), and the Tadpole galaxy UGC10214 (Tran et al. 2003) all have masses of $\sim 10^6 \mathrm{M}_\odot$, similar to those in HCG 31. However, all of these galaxies are 0.6 to 1.3 mag brighter than A+C, the brightest of the HCG 31 galaxies, so the HCG 31 complexes are more massive relative to their galaxy luminosity.

Another exceptional interacting system is Arp 285, which consists of two galaxies with a tidal tail containing beads of star-forming complexes observed with *Spitzer* (Smith et al. 2008). These galaxies are each ~ 0.8 magnitudes fainter than A+C; their tail clump masses are $< 10^6$ $\mathrm{M}_\odot$, but they also contain a bright spot in the disk with 10^8 $\mathrm{M}_\odot$.

3.7. *Comparison with Complexes in High Redshift Galaxies*

Complexes have been observed with *HST* in high redshift galaxies in the GEMS and GOODS fields (Elmegreen & Elmegreen 2006; Elmegreen et al. 2007a) and in the Ultra Deep Field (UDF; Elmegreen & Elmegreen 2005; Elmegreen et al. 2005, 2007b, 2008), with sizes in the kpc range. In the standard ΛCDM cosmology (Spergel et al. 2007), 1 kpc corresponds to $\sim 0\farcs13$ at $z = 1$, and has a nearly constant angular size over the redshift range $0.7 < z < 4$. At closer redshifts, the angular size decreases approximately linearly with increasing redshift. With $0\farcs03$ pixels in the ACS images, a kpc-size region corresponds to 3–4 pixels, so complexes much smaller than this could not be measured in the UDF galaxies. On the other hand, if there were complexes significantly larger than this in nearby galaxies, they would be easily discernible. In other words, the largest complexes can be identified and compared in both local and high redshift galaxies. The high z galaxy complexes have masses typically 10^7 to a few $10^8 M_\odot$ from $z = 1-4$, decreasing to about $10^6 \mathrm{M}_\odot$ at $z = 0.1-0.2$, as shown in detail in figures in the previous papers. For the high z cases, masses are estimated by comparing the complex position in color-magnitude space (cf. Fig. 5) and comparing with evolutionary tracks that span a range of reasonable star formation decay rates. In HCG 31, the masses are estimated by comparison with single population, instantaneous burst evolutionary models. Given the colors of the HCG 31 complexes, the inferred masses are not highly sensitive to this assumption which results in a factor of approximately two uncertainty (cf. Fig. 10, Elmegreen et al. 2007a).

Among just the obviously interacting galaxies, which include M51-type galaxies as well as strongly interacting, gas-rich pairs with long tidal arms (Elmegreen et al. 2007a), the complex masses are 10^5 to $10^{6.5}$ $\mathrm{M}_\odot$ at nearby redshifts up to $z = 0.125$, and $10^7 - 10^9 \mathrm{M}_\odot$ at redshifts $1 < z < 1.4$. Faint tidal features are difficult to discern at higher redshifts because of cosmological dimming.

In our GEMS and GOODS samples, galaxies at $z < 0.2$ mostly have rest-frame M_V fainter than –18, because the small volume covered to that depth does not include many intrinsically brighter galaxies; beyond $z = 0.2$, the galaxies we measured have rest-frame M_V from –18 to –22. As in local galaxies, the largest complexes are dependent on the absolute (rest-frame) magnitudes of the galaxies, so the main reason the lower redshift GEMS and GOODS complexes are less massive is because their host galaxies are intrinsically fainter. The largest complex masses have a spread of about a factor of 10 for a given absolute rest-frame magnitude, ranging from $\sim 10^{6.5} \mathrm{M}_\odot$ for rest-frame M_V of –16 to $\sim 10^8$ $\mathrm{M}_\odot$ for –20.5 mag (Elmegreen et al., in prep.). These masses are a factor of $\sim$10 larger for a given absolute magnitude than for complexes in local galaxies. In order to compare the complexes in HCG 31 with those in high redshift galaxies, a Gaussian blur of 30 was applied to the HCG 31 images, corresponding to pixels covering about 250 pc. This scale simulates its appearance if at $1 < z < 4$.

The HCG 31 complexes were re-measured based on their boundaries in the blurred images. Some complexes were not recognizable in the blurred images because they were too faint or too small; a few were blended with other complexes that were too close. Most of the lowest mass complexes disappear, although the remaining complexes still range from $\sim 10^5$ to $10^{7.3}$ $\mathrm{M}_\odot$. A comparison of the full resolution and blurred complexes shows that the blurred ones typically are only $\sim$20% more massive, even when they contain blended complexes; the colors differ by at most ~ 0.2 mag, so the inferred ages are about the same. The diameters range from about 300 to 650 pc (in one case, the diameter measured was smaller than in the unblurred image, due to uncertainty in placing the boundary.) These complexes are similar in mass and size to those in the interacting GEMS and GOODS galaxies of comparable rest-frame magnitudes.

The larger masses in the high redshift galaxies are presumed to be the result of high turbulence in the disks; for example, kinematics inferred from spectroscopic observations of a $z = 1.6$ galaxy, UDF6462, indicates velocity dispersions of 40 $\mathrm{km\,s^{-1}}$ (Bournaud et al. 2008), while numerical simulations reproducing the large scale star formation (Bournaud et al. 2007) also require values several times higher than in local quiescent galaxies.

Thus, the complexes in HCG 31 can be understood in terms of large-scale star formation from gravitational instabilities in the gas driven by turbulence. Their sizes are comparable to what is expected based on complexes in nearby spirals. Their masses are similar to those in $z \sim 1$ galaxies of comparable magnitude, and are intermediate between the smaller ones found in gently interacting nearby systems and the larger ones found in presumably more turbulent high redshift counterparts.

3.8. *Underlying Stellar Populations*

An outstanding issue from previous *HST* studies is whether F contains an older stellar population in addition to the current generation of young stars. From an examination of the region-specific color-color plot (Fig. 6), none of the star cluster candidates or complexes in F have colors consistent with > 1 Gyr populations, and there is only one globular cluster candidate within the larger F boundary. In general, it is hard to see individual, old stars directly (with the exception of GCs), due to their faintness. The diffuse light within galaxies offers an opportunity to study fainter stellar populations than those described in the previous sections and can give us a handle on the population of older stars.

To search for a distributed, underlying, older stellar population, we examined a processed B_{435}–I_{814} image of the entire ACS field of view. The image, presented in Figure 12, was created from the point-source subtracted images generated by the SC candidate PSF-fitting photometry. It has been Vega-magnitude calibrated and boxcar-smoothed (with a 13 pix [180 pc] window) and corrected for Galactic extinction. We use B_{435}–I_{814} to remove the confusion of nebular emission prominent in V_{606}, and also because B_{435}–$I_{814} \gtrsim 0.7$ is a good indicator of stellar populations with ages > 200 Myr, barring intrinsic reddening (see Figure 12).

In actively star forming galaxies, the diffuse light will be a mix of different stellar populations. We might expect the light to be dominated by the youngest (and also brightest) stars that are present. Therefore, we will typically be able to put a lower limit on the age of stars contributing to the diffuse light in the galaxies.

From inspection, diffuse tidal debris with B_{435}–I_{814}~0.4–0.8 apparently pulled out from A+C is evident to the north, as is some debris stretching to the south and overlapping with E and H. These colors are consistent with stellar ages > 100 Myr in this debris. The overall colors of A+C and B are in the range B_{435}–I_{814}=0.4–1.0, with bluer (B_{435}–I_{814}=–0.1 to 0.4) regions coincident with the locations of the youngest SC candidates. While the inner disk of G is blue (B_{435}–$I_{814} \sim 0.4$), the location of the complexes to the west stand out with B_{435}–I_{814}~–0.1 to 0.4. The outer disk of G is significantly redder than the other structures in the group, with B_{435}–I_{814}=0.7–1.2. From the B_{435}–I_{814} color-magnitude diagram this indicates that the intermediate age range in A+C, B, and G is at least several 100 Myr, up to ~ 1 Gyr. The presence of GC candidates (§3.4) also supports the presence of ancient stars in these galaxies.

Notably, F shows no evident diffuse emission consistent with an older stellar population; the reddest regions have B_{435}–$I_{814} \sim$ 0.2–0.3, consistent with stars < 10 Myr. Given the low surface brightness of this material, it cannot be hiding a substantial population of old stars. While we cannot rule out that there is some low level stellar population with ages of 100 Myr and older, these observations show no evidence for such a population, and probably give the best evidence to date that F started forming stars only recently. This implies that the material comprising F is almost entirely 'fresh', and F is overall a very young structure.

4. SUMMARY AND CONCLUSIONS

4.1. *Modes of Star Formation*

An in-depth examination of the colors of structures at all scales of star formation, from compact star cluster candidates, to large star-forming clusters, to the diffuse underlying emission, indicates that the entire HCG 31 system is suffused with recent and ongoing star formation. Star cluster candidates with nebular colors are present throughout HCG 31, specifically concentrated in the inner disk and western ring of G, through the midplane of B, in the interaction region of A+C, and across E, H, and F. While the prominence of SC candidates with nebular colors is not sufficient evidence of a recent enhancement of star formation activity, other available information points in that direction. In particular, while the SFR is enhanced relative to galaxies with similar masses, the sum total of H I in the system is not noticeably depleted. Crudely, this sets an upper limit to the timescale of enhanced star formation of ~ 400 Myr, as in this amount of time a significant fraction ($\sim 10\%$) of the H I would have been converted to stars. In simulations of mergers of pairs of bulgeless disk galaxies, the typical timescale for the SFR to be elevated by an order of magnitude or so is ~ 150 Myr, and the most intense burst is triggered shortly after the first encounter (Mihos & Hernquist 1996). If these results are applicable to the more complicated dynamics of the compact group environment, then the ongoing burst may be of quite recent vintage. The current high rate of star formation is not sustainable long term (at most a few Gyrs) given the finite reservoir of cold gas of 1.6×10^{10} $M_{\odot}$ (Verdes-Montenegro et al. 2005).

On the scales of star clusters, both young and globular, the HCG 31 system is consistent with local galaxies of similar star formation rates and masses, as shown by the luminosity functions (Figs. 4 and 10). Furthermore, the values of brightest cluster $M_{V_{606}}$ as a function of number for distinct regions in HCG 31 match those of galaxies in the local Universe with a range of properties (Fig. 8). This supports the claim that star cluster formation (and destruction) follow universal patterns that scale with star formation rate, but are otherwise insensitive to their large scale environment.

However, the SC candidate populations of all compact groups studied to date are not the same. Stephan's Quintet (HCG 92) is another Hickson Compact Group with active star formation as a result of strong gravitational interactions (e.g., Xu et al. 1999; Sulentic et al. 2001). Specifically, the galaxy NGC 7318b is blueshifted by 900 km s^{-1} with respect to the rest of the group galaxies, and is currently ploughing through the neutral intragroup medium (Shostak et al. 1984). This has triggered a large scale (~ 40 kpc) ridge of star formation coincident with a radio and X-ray bright shock (e.g., van der Hulst & Rots 1981; Pietsch et al. 1997; Trinchieri et al. 2003). With *HST* WFPC2 three-color imaging, Gallagher et al. (2001) identified a population of young, luminous SC candidates that traces the large scale shock. In contrast to HCG 31, however, none of these SC candidates has colors consistent with nebular emission, though clusters apparently as young as $\sim$ 2–3 Myr are seen. After accounting for the brighter absolute magnitude limit and different filters of the WFPC2 observations, SC candidates in Stephan's Quintet with comparable colors and absolute magnitudes (of $M_{\rm V} < -10$) to those in HCG 31 would have been detected if present. There are in total $\sim$ 30 star cluster candidates in Stephan's Quintet with comparably young ages ($\tau \lesssim 10$ Myr), the vast majority of which lie along the large-scale shock. From *Spitzer* spectroscopy of the shock ridge, strong, broad H_2 emission lines, weak polycyclic aromatic hydrocarbon emission, and very low excitation ionized gas tracers speak to the unusual environment of the region (Appleton et al. 2006). This setting may be one in which the interstellar medium of young clusters is rapidly stripped, and thus young clusters do not have cocoons of gas to photoionize.

On the kiloparsec scales of complexes, HCG 31 hosts a population with masses that more closely resemble those found at higher redshifts. This suggests that, similar to galaxies at $z = 1$–2 with similar absolute magnitudes, the disks of galaxies in HCG 31 have higher turbulent velocities than typically found in the local universe. This most plausibly arises because of the ongoing multigalaxy interactions in the system. In this sense therefore, the larger scale star formation structures are reminiscent of those seen during the epoch of morphological galaxy transformations in dense environments.

4.2. *Dwarf Galaxy Candidates*

Previous optical photometry suggested that galaxy F, composed of two separate H I peaks within the same cloud, is comprised of only a young population and that given its location in the tidal tail of the A+C complex it is likely a recently formed structure undergoing its first burst of star formation (Johnson & Conti 2000). Richer et al. (2003) find that galaxies E and F have similar oxygen abundances to A+C, verifying that they have been tidally removed from the A+C complex. The stellar populations are younger than the travel time from the A+C complex, and clearly are forming *in situ* (Mendes de Oliveira et al. 2006).

Amram et al. (2004, 2007) found a flat / shallow rotation velocity in E and F using optical Fabry-Perot data, and thus classify them as tidal debris though dwarf galaxies are expected to be slow rotators (Mendes de Oliveira et al. 2006). While E and H are merely fragments which are likely to fall back into A+C, F and R have H I column densities and Hα luminosities consistent with being true dwarf galaxies, and given their positions it is unlikely that they will fall back into the A+C complex.

To search for extended sources that might be identified with either tidal dwarf galaxy candidates or dissolved clusters, we ran the `SExtractor` software package (Bertin & Arnouts 1996) four times, each time with a different background smoothing size, which typically favors objects of different sizes. After merging the catalogs, multiple detections were combined. The 'best' detection was chosen to be (in order) the roundest, biggest, and least stellar source. By visual inspection of the extended sources (particularly in the tidal debris of E, F, and H) identified by these means, no obvious dwarf galaxy candidates were evident. The majority of the most significant candidates can be identified either with the complexes or marginally resolved SC candidates. Furthermore, the B_{435}–V_{606} and V_{606}–I_{814} color distributions of the `SExtractor` sources were consistent with these populations.

From the colors and luminosities of the SC candidates and complexes, the total stellar mass in F is $\gtrsim 10^6 {\rm M}_\odot$. While this is within the range found for dwarf galaxies, it is unclear whether it is sufficient to establish F as an independent entity within this compact group. From our analysis of the faint, diffuse emission in F, we find no evidence for an older stellar population, consistent with the Johnson & Conti (2000) analysis.

4.3. *Future Evolution*

The multiple interactions of low mass galaxies that characterize the HCG 31 system are evocative of hierarchical structure formation in process, and so we consider the likely end result, and compare it to early type systems in the local Universe that presumably underwent this type of dynamical processing at earlier times ($z \gtrsim 1$). We thus examine if HCG 31 can be cast accurately as a high-redshift analog.

At present, the sum of H I in HCG 31 as a whole is consistent with that expected from its member galaxies based on their magnitudes and morphologies (Williams et al. 1991; Verdes-Montenegro et al. 2001), though a large fraction of that gas has been pulled out from the individual galaxies into tidal structures. This suggests that HCG 31 has recently contracted as the gas has not yet been significantly reduced by a long period of star formation. The low radial velocity dispersions of the five primary galaxies (A, B, C, G, and Q) and the projected lengths of the H I tails are generally consistent with a bound system (Mendes de Oliveira et al. 2006). It seems quite likely that the individual galaxies in this group will ultimately merge into a single elliptical, as predicted by Rubin et al. (1990), in a wet merger process. Subsequently, it is not likely to move along the red sequence to higher luminosities as there are no candidates for future dry mergers in the neighborhood. We then consider whether this system will become a so-called 'fossil group': the putative remnant of a coalesced compact group.

A key component of the fossil group definition is a hot, extended X-ray medium with $L_{\rm X} \geq 0.5 \times 10^{42} h_{70}^{-2}$ erg s^{-1} (Jones et al. 2003). At present, HCG 31 has little extended X-ray emission. Unlike in galaxy clusters, the kinetic energy in the galaxies themselves is not sufficient to collisionally heat gas to X-ray-emitting temperatures. Therefore, the only possible source of heating is star formation whereby the mechanical energy from supernovae and stellar winds is thermalized into $\sim 10^6$ K gas. We can make a crude estimate of the potential X-ray luminosity (excluding compact sources) generated by conversion of the available reservoir of neutral gas into stars. In the following argument, we use the numbers from Mihos & Hernquist (1996) for the efficiencies of gas-to-star and supernova-to-kinetic energy conversions. If 75% of the $1.6 \times 10^{10} {\rm M}_\odot$ of H I is converted to stars, then $\sim 9 \times 10^7$ supernovae are expected assuming the initial mass function of §2.4. If 10^{-4} is the fraction of supernova energy converted to kinetic energy, and all of that energy is ultimately radiated as X-rays, the integrated X-ray energy of all supernova (assuming $E_{\rm SN} = 10^{51}$ ergs) is 9×10^{54} ergs. Over the course of a 150 Myr star formation episode, the power would thus be 2×10^{39} erg s^{-1}, or approximately 0.4% of the minimum for a fossil group. However, the total dynamical (including dark matter) mass of HCG 31 from H I velocities (assuming spherical symmetry and dynamical relaxation; Verdes-Montenegro et al. 2005) is 2×10^{11} M$_\odot$, approximately two orders of magnitude smaller than the dark matter halo mass of the lower mass (and lower X-ray luminosity) fossil groups (e.g., Díaz-Giménez et al. 2008). Therefore, HCG 31 is a plausible candidate for a low mass fossil group, where fossil group here applies to the dynamical history of a system rather than the specific X-ray luminosity criteria as defined by Jones et al. (2003).

We can also consider the current population of globular clusters, and investigate how that compares to those of low mass ellipitical galaxies in the local universe. While our value of $S_{\rm N} = 0.6$ for a galaxy with $M_{\rm V} = -20.7$ ($L_{\rm V} = 1.6 \times 10^9 {\rm L}_\odot$) would be low for an elliptical of this absolute magnitude, late type galaxies have higher mass-to-light ratios, and therefore lower values of $S_{\rm N}$ even with the same number of clusters per unit mass. A globular cluster system studied previously in NGC 6868, an E2 galaxy in the Telescopium group ($\sigma \sim 250$ km s^{-1}) with evidence of somewhat recent merger activity, has $S_{\rm N} = 1.1$, a value on the low end for ellipticals (Da Rocha et al. 2002a). Could such a galaxy be the result of a coalesced HCG 31?

To compare globular system in galaxies of different type, it is more convenient to use the T parameter, defined as the number of old globular clusters per unit mass (Zepf & Ashman 1993). Assuming values of $M/L_{\rm V}$=10 and 3 for ellipticals and late-type spirals, respectively, we obtain $T = 1.7 \pm 0.8$ for HCG 31 assuming a total globular cluster population of 111 ± 51 for the entire system and a mass of 6×10^{10} M$_\odot$. The corresponding T value for NGC 6868 ($M_{\rm V} = -21.9$; $L_{\rm V} = 5 \times 10^{10}$ L$_\odot$; $M = 49 \times 10^{10}$ M$_\odot$) using the globular cluster numbers from Da Rocha et al. (2002a) is 2.2 ± 1.1. Using $M_{\rm V} = -22.17$ (Forbes et al. 2007) for NGC 6868 gives $T = 1.7 \pm 0.9$. Therefore, correcting for the differing mass-to-light ratios of the two systems makes them fully consistent within the uncertainties. Note that the T value for HCG 31 would likely be a lower limit, given that it is currently forming new star clusters, some with masses $\gtrsim 10^5 {\rm M}_\odot$(see Fig. 7); these massive clusters would only increase the T value if they survive the next few Gyrs intact.

In sum, the likely outcome is that HCG 31 will have too low a mass and insufficient X-ray luminosity to meet the Jones et al. (2003) criteria for classification as a fossil group at $z = 0$. However, in terms of dynamical evolution and $L_{\rm X}$ vs. halo mass, it could plausibly extend the relation seen in fossil groups to lower masses. The globular cluster populations of local ellipticals of similar mass to HCG 31, however, are consistent with the current population of globular clusters in HCG 31 even if the ongoing star formation does not boost their numbers. HCG 31 therefore does enable us to investigate hierarchical structure formation such as occurred at higher redshift in a local setting, though the likely result will be a smaller version of the end products of group coalescence that currently exist in the local Universe.

This research was supported by grant xxx-xxx from the Space Telescope Science Institute and the National Science and Engineering Research Council of Canada (SCG).

REFERENCES

Amram, P., Mendes de Oliveira, C., Plana, H., Balkowski, C., & Hernandez, O. 2007, A&A, 471, 753
Amram, P., et al. 2004, ApJ, 612, L5
Appleton, P. N., et al. 2006, ApJ, 639, L51, arXiv:astro-ph/0602554
Balogh, M. L., Baldry, I. K., Nichol, R., Miller, C., Bower, R., & Glazebrook, K. 2004, ApJ, 615, L101, arXiv:astro-ph/0406266
Barkhouse, W. A., West, M. J., & Bothun, G. D. 2001, ApJ, 562, 679, arXiv:astro-ph/0107491
Bertin, E. & Arnouts, S. 1996, A&AS, 117, 393
Bournaud, F., Elmegreen, B. G., & Elmegreen, D. M. 2007, ApJ, 670, 237, arXiv:0708.0306
Bournaud, F., et al. 2008, A&A, 486, 741, arXiv:0803.3831
Brodie, J. P. & Strader, J. 2006, ARA&A, 44, 193, arXiv:astro-ph/0602601
Bruzual, G. & Charlot, S. 2003, MNRAS, 344, 1000
Calzetti, D., et al. 2007, ApJ, 666, 870, 0705.3377
Cardelli, J. A., Clayton, G. C., & Mathis, J. S. 1989, ApJ, 345, 245
Chandar, R., Fall, S. M., & Whitmore, B. C. 2006, ApJ, 650, L111, arXiv:astro-ph/0609360
Chandar, R., Whitmore, B., & Lee, M. G. 2004, ApJ, 611, 220, arXiv:astro-ph/0407460
Chromey, F. R., Elmegreen, D. M., Mandell, A., & McDermott, J. 1998, AJ, 115, 2331
Conti, P. S. 1991, ApJ, 377, 115
Conti, P. S., Leitherer, C., & Vacca, W. D. 1996, ApJ, 461, L87+, arXiv:astro-ph/9602084
Cooper, M. C., et al. 2007, MNRAS, 376, 1445, arXiv:astro-ph/0607512
Cucciati, O., et al. 2006, A&A, 458, 39
Da Rocha, C., de Oliveira, C. M., Bolte, M., Ziegler, B. L., & Puzia, T. H. 2002a, AJ, 123, 690
Da Rocha, C. & Mendes de Oliveira, C. 2005, MNRAS, 364, 1069, arXiv:astro-ph/0509908
Da Rocha, C., Mendes de Oliveira, C., Bolte, M., Ziegler, B. L., & Puzia, T. H. 2002b, AJ, 123, 690
Da Rocha, C., Ziegler, B. L., & Mendes de Oliveira, C. 2008, MNRAS, 388, 1433, 0805.4015
Díaz-Giménez, E., Muriel, H., & Mendes de Oliveira, C. 2008, A&A, 490, 965, 0809.2290
Dopita, M. A., Pereira, M., Kewley, L. J., & Capaccioli, M. 2002, ApJS, 143, 47
Dressler, A. 1980, ApJ, 236, 351
Dressler, A., et al. 1997, ApJ, 490, 577
Efremov, Y. N. 1995, AJ, 110, 2757
Elmegreen, B. G. & Elmegreen, D. M. 2005, ApJ, 627, 632, arXiv:astro-ph/0504032
Elmegreen, B. G., Elmegreen, D. M., Salzer, J. J., & Mann, H. 1996, ApJ, 467, 579
Elmegreen, B. G., Kaufman, M., & Thomasson, M. 1993, ApJ, 412, 90
Elmegreen, D., Elmegreen, B., Fernandez, M., & Lemonias, J. 2008, ApJ, submitted
Elmegreen, D. M., Chromey, F. R., Knowles, B. D., & Wittenmyer, R. A. 1998, AJ, 115, 1433
Elmegreen, D. M. & Elmegreen, B. G. 2006, ApJ, 651, 676, arXiv:astro-ph/0607579
Elmegreen, D. M., Elmegreen, B. G., Ferguson, T., & Mullan, B. 2007a, ApJ, 663, 734, arXiv:0704.0911

Elmegreen, D. M., Elmegreen, B. G., Kaufman, M., Sheth, K., Struck, C., Thomasson, M., & Brinks, E. 2006, ApJ, 642, 158, arXiv:astro-ph/0605524

Elmegreen, D. M., Elmegreen, B. G., Lang, C., & Stephens, C. 1994, ApJ, 425, 57

Elmegreen, D. M., Elmegreen, B. G., Ravindranath, S., & Coe, D. A. 2007b, ApJ, 658, 763

Elmegreen, D. M., Elmegreen, B. G., Rubin, D. S., & Schaffer, M. A. 2005, ApJ, 631, 85, arXiv:astro-ph/0508216

Elmegreen, D. M., Kaufman, M., Elmegreen, B. G., Brinks, E., Struck, C., Klarić, M., & Thomasson, M. 2001, AJ, 121, 182

Elmegreen, D. M. & Salzer, J. J. 1999, AJ, 117, 764

Fall, S. M., Chandar, R., & Whitmore, B. C. 2005, ApJ, 631, L133, arXiv:astro-ph/0509293

Forbes, D. A., Proctor, R., Strader, J., & Brodie, J. P. 2007, ApJ, 659, 188, arXiv:astro-ph/0612415

Franzetti, P., et al. 2007, A&A, 465, 711, arXiv:astro-ph/0607075

Gallagher, S. C., Charlton, J. C., Hunsberger, S. D., Zaritsky, D., & Whitmore, B. C. 2001, AJ, 122, 163

Gallagher, S. C., Johnson, K. E., Hornschemeier, A. E., Charlton, J. C., & Hibbard, J. E. 2008, ApJ, 673, 730

Gooch, R. 1996, in Astronomical Data Analysis Software and Systems V, eds. G. H. Jacoby & J. Barnes, vol. 101 of *Astronomical Society of the Pacific Conference Series*, 80–+

Goudfrooij, P., Strader, J., Brenneman, L., Kissler-Patig, M., Minniti, D., & Edwin Huizinga, J. 2003, MNRAS, 343, 665, arXiv:astro-ph/0304195

Harris, W. E. 1996, AJ, 112, 1487

— 2001, in Saas-Fee Advanced Course 28: Star Clusters, eds. L. Labhardt & B. Binggeli, 223–+

Harris, W. E. & van den Bergh, S. 1981, AJ, 86, 1627

Hickson, P. 1993, Astrophysical Letters Communications, 29, 1

Hickson, P., Mendes de Oliveira, C., Huchra, J. P., & Palumbo, G. G. 1992, ApJ, 399, 353

Hogg, D. W., et al. 2004, ApJ, 601, L29, arXiv:astro-ph/0307336

Iglesias-Paramo, J. & Vilchez, J. M. 1997, ApJ, 479, 190

Johnson, K. E. & Conti, P. S. 2000, AJ, 119, 2146

Johnson, K. E., Hibbard, J. E., Gallagher, S. C., Charlton, J. C., Hornschemeier, A. E., Jarrett, T. H., & Reines, A. E. 2007, AJ, 134, 1522

Johnson, K. E., Vacca, W. D., Leitherer, C., Conti, P. S., & Lipscy, S. J. 1999, AJ, 117, 1708

Jones, L. R., Ponman, T. J., Horton, A., Babul, A., Ebeling, H., & Burke, D. J. 2003, MNRAS, 343, 627, arXiv:astro-ph/0304257

Kennicutt, R. C., Jr. 1998, ARA&A, 36, 189

Kunth, D. & Schild, H. 1986, A&A, 169, 71

Lada, C. J. & Lada, E. A. 2003, ARA&A, 41, 57, arXiv:astro-ph/0301540

Larsen, S. S. 2002, AJ, 124, 1393, arXiv:astro-ph/0206295

Leitherer, C., et al. 1999, ApJS, 123, 3

López-Sánchez, Á. R. & Esteban, C. 2007, ArXiv e-prints, 0704.2846

López-Sánchez, Á. R., Esteban, C., & Rodríguez, M. 2004, ApJS, 153, 243

Maraston, C. 2005, MNRAS, 362, 799, arXiv:astro-ph/0410207

Mendes de Oliveira, C. L., Temporin, S., Cypriano, E. S., Plana, H., Amram, P., Sodré, L. J., & Balkowski, C. 2006, AJ, 132, 570

Meyer, M. J., et al. 2004, MNRAS, 350, 1195

Mihos, J. C. & Hernquist, L. 1996, ApJ, 464, 641, arXiv:astro-ph/9512099

Mirabel, I. F., Dottori, H., & Lutz, D. 1992, A&A, 256, L19

Pietsch, W., Trinchieri, G., Arp, H., & Sulentic, J. W. 1997, A&A, 322, 89

Pildis, R. A., Bregman, J. N., & Schombert, J. M. 1995, AJ, 110, 1498, arXiv:astro-ph/9507039

Rector, T. A., Levay, Z. G., Frattare, L. M., English, J., & Pu'uohau-Pummill, K. 2007, AJ, 133, 598, arXiv:astro-ph/0412138

Rejkuba, M., Greggio, L., Harris, W. E., Harris, G. L. H., & Peng, E. W. 2005, ApJ, 631, 262

Rhode, K. L. & Zepf, S. E. 2001, AJ, 121, 210

— 2004, AJ, 127, 302

Rhode, K. L., Zepf, S. E., Kundu, A., & Larner, A. N. 2007, AJ, 134, 1403

Richer, M. G., Georgiev, L., Rosado, M., Bullejos, A., Valdez-Gutiérrez, M., & Dultzin-Hacyan, D. 2003, A&A, 397, 99, arXiv:astro-ph/0211033

Robin, A. C., Reylé, C., Derrière, S., & Picaud, S. 2003, A&A, 409, 523, arXiv:astro-ph/0401052

Rubin, V. C., Hunter, D. A., & Ford, W. K. J. 1990, ApJ, 365, 86

Salzer, J. J., Jangren, A., Gronwall, C., Werk, J. K., Chomiuk, L. B., Caperton, K. A., Melbourne, J., & McKinstry, K. 2005, AJ, 130, 2584

Schlegel, D. J., Finkbeiner, D. P., & Davis, M. 1998, ApJ, 500, 525, arXiv:astro-ph/9710327

Schweizer, F. 1978, in Structure and Properties of Nearby Galaxies, eds. E. M. Berkhuijsen & R. Wielebinski, vol. 77 of *IAU Symposium*, 279–284

Selman, F. J. & Melnick, J. 2000, ApJ, 534, 703

Shostak, G. S., Allen, R. J., & Sullivan, W. T., III 1984, A&A, 139, 15

Sirianni, M., et al. 2005, PASP, 117, 1049

Smith, B. J., et al. 2008, AJ, 135, 2406, 0803.4218

Spergel, D. N., et al. 2007, ApJS, 170, 377

Stetson, P. B. 1987, PASP, 99, 191

Sulentic, J. W., Rosado, M., Dultzin-Hacyan, D., Verdes-Montenegro, L., Trinchieri, G., Xu, C., & Pietsch, W. 2001, AJ, 122, 2993

Tran, H. D., et al. 2003, ApJ, 585, 750, arXiv:astro-ph/0211371

Trinchieri, G., Sulentic, J., Breitschwerdt, D., & Pietsch, W. 2003, A&A, 401, 173

Vacca, W. D. & Conti, P. S. 1992, ApJ, 401, 543

van der Hulst, J. M. & Rots, A. H. 1981, AJ, 86, 1775

Verdes-Montenegro, L., Del Olmo, A., Yun, M. S., & Perea, J. 2005, A&A, 430, 443

Verdes-Montenegro, L., Yun, M. S., Williams, B. A., Huchtmeier, W. K., Del Olmo, A., & Perea, J. 2001, A&A, 377, 812

Vicari, A., Battinelli, P., Capuzzo-Dolcetta, R., Wyder, T. K., & Arrabito, G. 2002, A&A, 384, 24

Wetzstein, M., Naab, T., & Burkert, A. 2007, MNRAS, 375, 805, arXiv:astro-ph/0510821

White, P. M., Bothun, G., Guerrero, M. A., West, M. J., & Barkhouse, W. A. 2003, ApJ, 585, 739

Whitmore, B. C. 2003, in A Decade of Hubble Space Telescope Science, eds. M. Livio, K. Noll, & M. Stiavelli, 153–178

Whitmore, B. C., Chandar, R., & Fall, S. M. 2007, AJ, 133, 1067, arXiv:astro-ph/0611055

Whitmore, B. C., Zhang, Q., Leitherer, C., Fall, S. M., Schweizer, F., & Miller, B. W. 1999, AJ, 118, 1551

Whitmore, B. C., et al. 2005, AJ, 130, 2104

Williams, B. A., McMahon, P. M., & van Gorkom, J. H. 1991, AJ, 101, 1957

Williams, B. A. & Rood, H. J. 1987, ApJS, 63, 265

Willmer, C. N. A., et al. 2006, ApJ, 647, 853, arXiv:astro-ph/0506041

Xu, C., Sulentic, J. W., & Tuffs, R. 1999, ApJ, 512, 178

Zepf, S. E. & Ashman, K. M. 1993, MNRAS, 264, 611

TABLE 1
Star Cluster and Globular Cluster Candidate Data[a]

Region	$N_{\rm comp}$[b]	$N_{\rm SCCs}$[c]	$f_{\rm neb}$[d]	$M_{\rm V_{606}}$(brightest)	$N_{\rm GCCs}$[e]	S_N[f]	$M_{\rm B_{435}}$	$B-V$[g]
A+C	11	178	0.29	–15.5	50 ± 26	0.5 ± 0.3	–20.0	0.03
B	11	105	0.23	–13.4	39 ± 22	1.3 ± 0.7	–18.5	0.17
E	3	17	0.35	–11.6	(3)	(0.3)	–16.5	–0.03
F	4	16	0.75	–11.4	(3)	(0.5)	–15.8	–0.08
G	11	86	0.33	–13.4	20 ± 13	0.6 ± 0.4	–18.9	–0.01
H	0	3	0.67	–11.2	0	0	···	···

[a]None of the values in this table has been corrected for intrinsic extinction.
[b]Number of complexes in each region (see §2.3).
[c]Number of star cluster candidates in each region (see §2.1).
[d]Fraction of star cluster candidates in each region with colors consistent with nebular emission (see §2.1 and the lefthand panel of Fig. 5).
[e]Total calculated number of globular cluster candidates after correction for incompleteness (see §3.4). Numbers in parentheses were estimated from only one object.
[f]Specific frequency of globular cluster candidates (see §3.4). Numbers in parentheses were calculated from one object.
[g]From Table 2 of López-Sánchez et al. (2004).

TABLE 2
Star-forming Complexes

Region	Complex	RA	Dec	$M_{V_{606}}$	B_{435}–V_{606}	V_{606}–I_{814}	Diameter (pc)
A+C	1	5:01:39.7676	-4:15:11.865	−14.09	0.31	0.23	539
A+C	2	5:01:38.6204	-4:15:14.205	−13.25	0.25	0.47	331
A+C	3	5:01:38.4399	-4:15:13.545	−13.88	0.26	0.16	452
A+C	4	5:01:38.0909	-4:15:24.225	−14.75	0.20	0.26	414
A+C	5	5:01:38.7127	-4:15:32.985	−15.37	0.47	0.64	306
A+C	6	5:01:38.2434	-4:15:33.285	−15.20	0.41	0.38	271
A+C	7	5:01:37.7319	-4:15:32.715	−15.81	0.85	−0.38	198
A+C	8	5:01:37.6858	-4:15:32.745	−14.71	0.60	−0.09	191
A+C	9	5:01:37.8062	-4:15:27.945	−17.73	0.51	−0.21	489
A+C	10	5:01:37.7500	-4:15:28.965	−15.77	0.36	−0.00	265
A+C	11	5:01:37.7019	-4:15:31.305	−17.01	0.27	−0.04	418
B	1	5:01:34.7918	-4:16:00.254	−14.34	0.38	−0.12	288
B	2	5:01:35.3112	-4:15:47.414	−13.71	0.32	0.39	274
B	3	5:01:35.2350	-4:15:50.534	−13.06	0.47	0.20	166
B	4	5:01:35.5840	-4:15:41.834	−13.52	0.51	0.18	265
B	5	5:01:35.8327	-4:15:40.334	−13.84	0.62	−0.21	265
B	6	5:01:35.7685	-4:15:40.154	−13.00	0.43	0.10	207
B	7	5:01:35.8327	-4:15:42.614	−12.54	0.77	−0.31	133
B	8	5:01:35.9169	-4:15:42.314	−13.34	0.31	0.18	257
B	9	5:01:35.7966	-4:15:44.114	−12.50	0.27	0.42	166
B	10	5:01:34.9863	-4:15:55.874	−13.08	0.34	0.47	248
B	11	5:01:35.2150	-4:15:51.974	−13.57	0.35	0.34	208
E	1	5:01:37.7058	-4:15:57.405	−13.47	0.40	0.04	299
E	2	5:01:37.5314	-4:15:56.715	−15.80	0.20	0.36	875
E	3	5:01:37.2887	-4:15:48.075	−12.89	0.36	−0.00	277
F	4	5:01:39.8016	-4:16:21.525	−15.11	0.83	−0.63	550
F	5	5:01:39.8598	-4:16:22.515	−13.60	0.38	−0.24	333
F	6	5:01:40.1947	-4:16:26.835	−14.27	0.67	−0.47	373
F	7	5:01:40.2589	-4:16:28.755	−12.48	0.36	−0.30	286
G	1	5:01:44.0455	-4:17:21.045	−14.68	0.31	0.41	252
G	2	5:01:43.9492	-4:17:20.985	−14.83	0.34	0.41	298
G	3	5:01:43.9212	-4:17:22.665	−13.89	0.45	−0.01	190
G	4	5:01:43.8610	-4:17:22.305	−13.86	0.37	−0.01	187
G	5	5:01:43.7687	-4:17:19.245	−13.98	0.36	0.21	214
G	6	5:01:43.7206	-4:17:19.485	−13.06	0.17	0.15	139
G	7	5:01:43.6685	-4:17:17.625	−15.05	0.63	−0.23	307
G	8	5:01:43.8289	-4:17:14.445	−15.30	0.38	0.17	407
G	9	5:01:43.9011	-4:17:14.085	−14.99	0.49	−0.00	357
G	10	5:01:43.9492	-4:17:15.105	−13.50	0.32	0.37	198
G	11	5:01:44.0816	-4:17:13.965	−13.58	0.26	0.20	184

TABLE 3
STAR FORMATION RATES

Region	L_{24} ($\log(\mathrm{erg\ s^{-1}\ Hz^{-1}})$)	SFR ($\mathrm{M_\odot\ yr^{-1}}$)
A+C+E	30.29	3.20
B	28.84	0.17
F	28.06	0.03
G	29.21	0.35
Q	27.46	0.01
Total	30.34	3.76

Fig. 1.— A five-color composite image of HCG 31 composed of purple (NUV *GALEX*), blue (B_{435} *HST*), yellow-green (V_{606} *HST*), orange (8 μm *Spitzer*), and red (I_{814} *HST*) images; see S 2.7. Group galaxies and tidal debris are labeled in light gray; HCG 31D (the red spiral in the upper right) is in the background. Young, massive stars are evident in blue and purple, and dust emission shows up as light orange. The brightest nebular emission regions glow pink, because they have both strong UV and dust emission. However, emission regions in which the UV and IR are less pronounced appear turquoise due to H_α emission falling within the wide V_{606}. The $30''$ scale corresponds to roughly 8 kpc. North is up, and east is to the left.

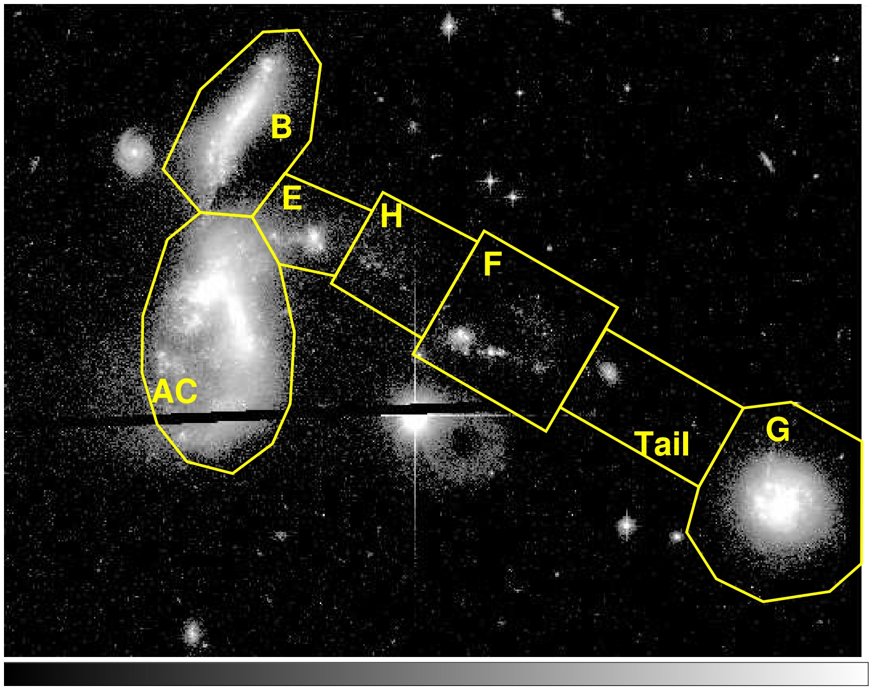

Fig. 2.— ACS V_{606} image of HCG 31. The yellow polygons denote the boundaries of the physical regions associated with the galaxies and tidal structures in HCG 31 as labeled. (● This will be replaced with a three-color *HST* image with the boundaries indicated.)

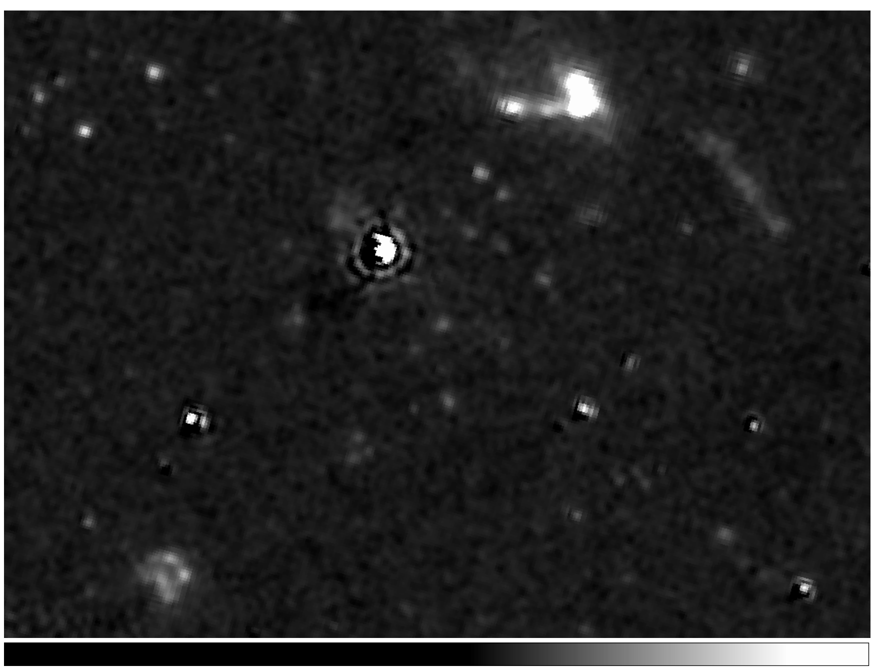

Fig. 3.— *Spitzer* 4.5μm image divided by the 3.6μm image scaled to emphasize the near-infrared emission in excess of that from stellar photospheres attributable to warm dust. The A+C overlap region is most prominent, and the assymmetry in G emphasizes the star-forming western side of the disk. The tidal debris is almost invisible, and B is quite faint. IRAC images from Johnson et al. (2007). (● This image might get nixed if the 5-color image shows the same thing.)

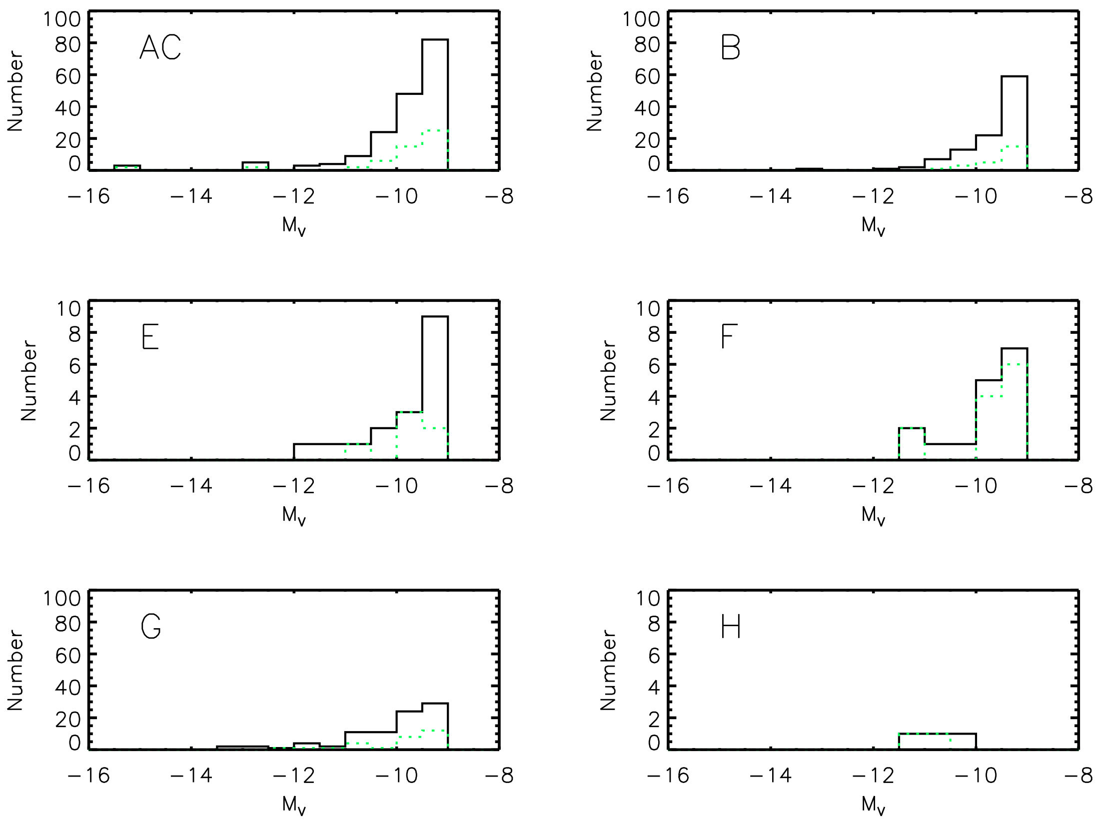

FIG. 4.— In each panel, the M_V distributions of star cluster candidates for the region as labeled. Dotted green histograms represent the distribution for SC candidates with nebular colors (see caption to Figure 5).

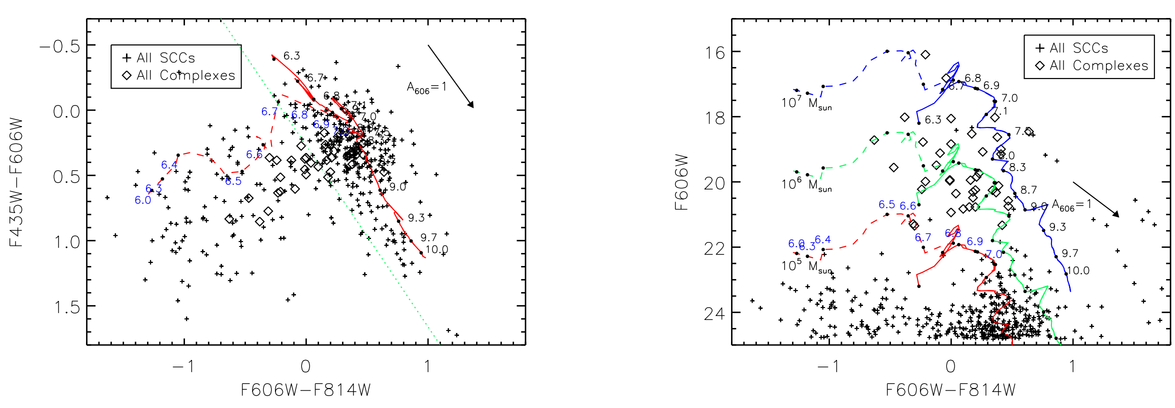

FIG. 5.— *(Left:)* B_{435}–V_{606} vs. V_{606}–I_{814} color-color plots of the star cluster candidates (SC candidates; crosses) and complexes (open diamonds) for the entire ACS field of view of HCG 31. The solid, red curve is a (Bruzual & Charlot 2003) evolutionary track for an instantaneous burst with 1/5 solar metallicity and a Salpeter initial mass function. The dashed curve includes evolutionary tracks which include nebular emission as described in section §2.4. SC candidates and complexes to the left of the dotted green line are considered to have nebular colors. *(Right:)* A V_{606} vs. V_{606}–I_{814} color-magnitude diagram for the SC candidates (crosses) and complexes (open diamonds). The evolutionary tracks for 10^5, 10^6, and 10^7 $M_\odot$ clusters are indicated with the curves as labeled; dashed curves include nebular emission. In both panels, Galactic extinction of $A_{F606W} = 1$ has been indicated with a labeled vector, and log(ages) in years are marked.

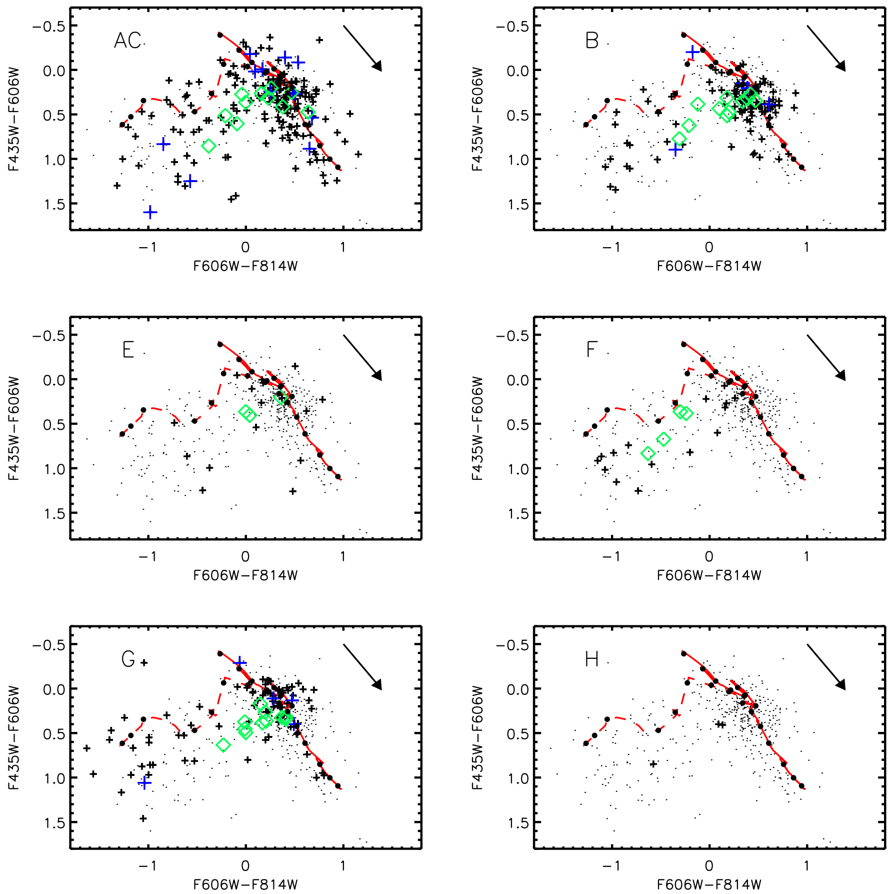

FIG. 6.— B_{435}–V_{606} vs. V_{606}–I_{814} color-color plots of the SC candidates and complexes in HCG 31. In each panel, black dots indicate all candidates with $M_{V_{606}} < -9$ from the entire ACS field of view, black crosses represent candidates within the region as labeled and shown in Figure 2. Larger, blue symbols are the most luminous SC candidates with $M_{V_{606}} < -11$, and open green diamonds are the complexes. Evolutionary tracks and reddening vectors are as described in the caption to Figure 5

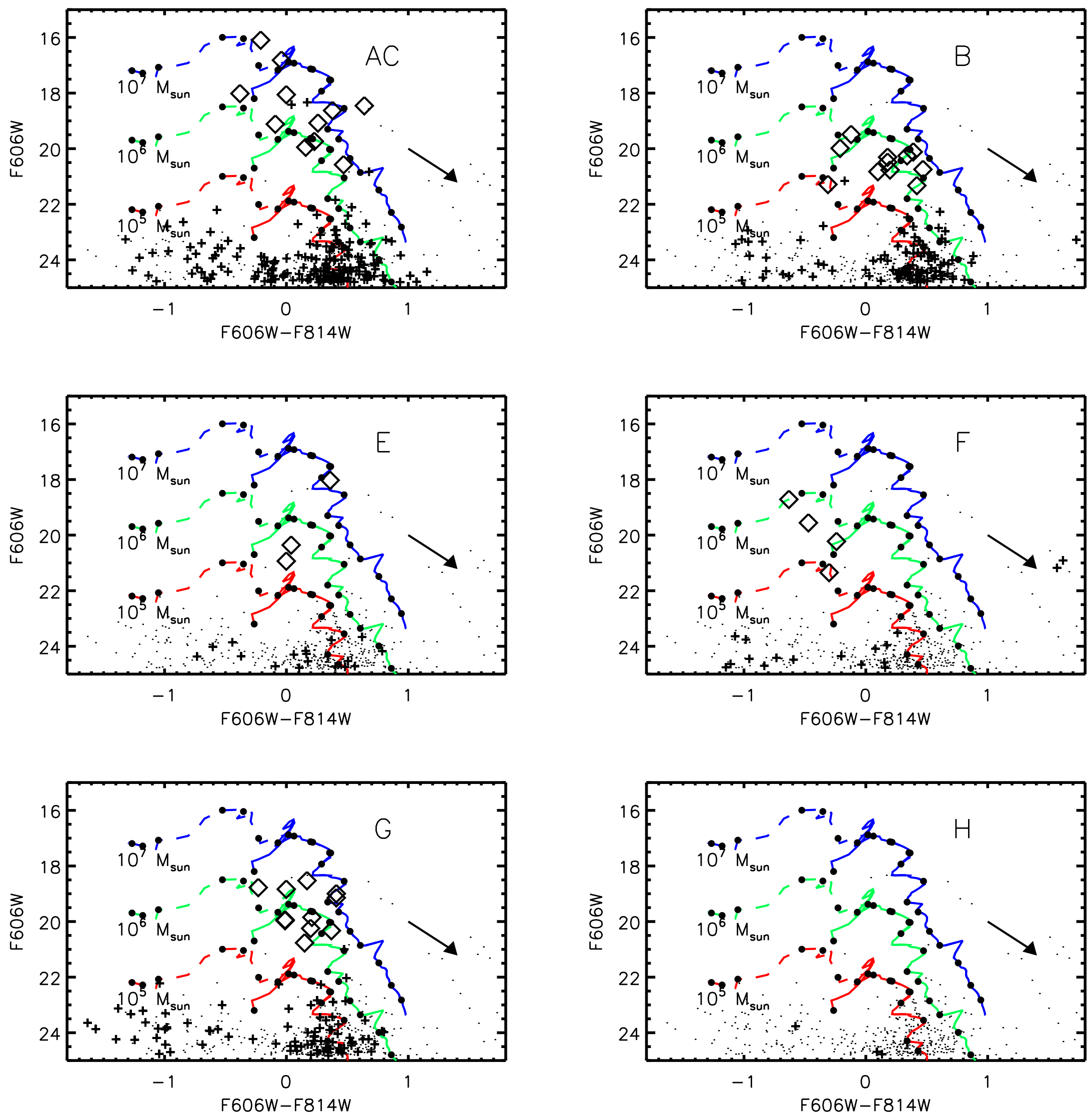

Fig. 7.— V_{606} vs. V_{606}–I_{814} color-magnitude plots of the SC candidates and complexes in HCG 31. In each panel, black dots indicate all candidates with $M_{\mathrm{V}_{606}} < -9$ from the entire ACS field of view, black crosses represent candidates within the region as labeled and shown in Figure 2, and open green diamonds are the complexes. Evolutionary tracks and reddening vectors are as described in the caption to Figure 5

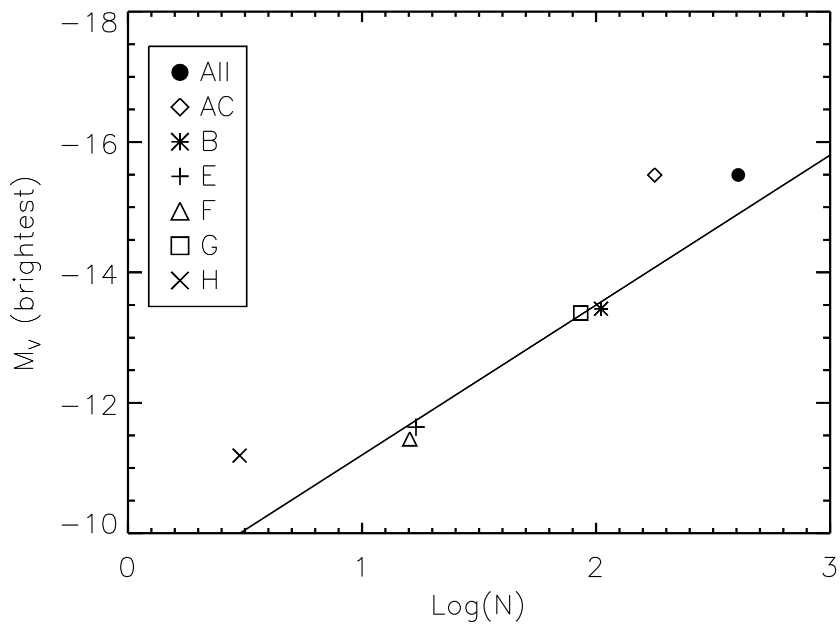

FIG. 8.— Brightest $M_{V_{606}}$ vs. log(N) (where N is the number of star cluster candidates brighter than $M_{V_{606}} = -9$) for the entire ACS field and each region as labeled in the legend. The solid line is the best-fitting value from Figure 11 of Whitmore et al. (2007) for 40 local star-forming galaxies.

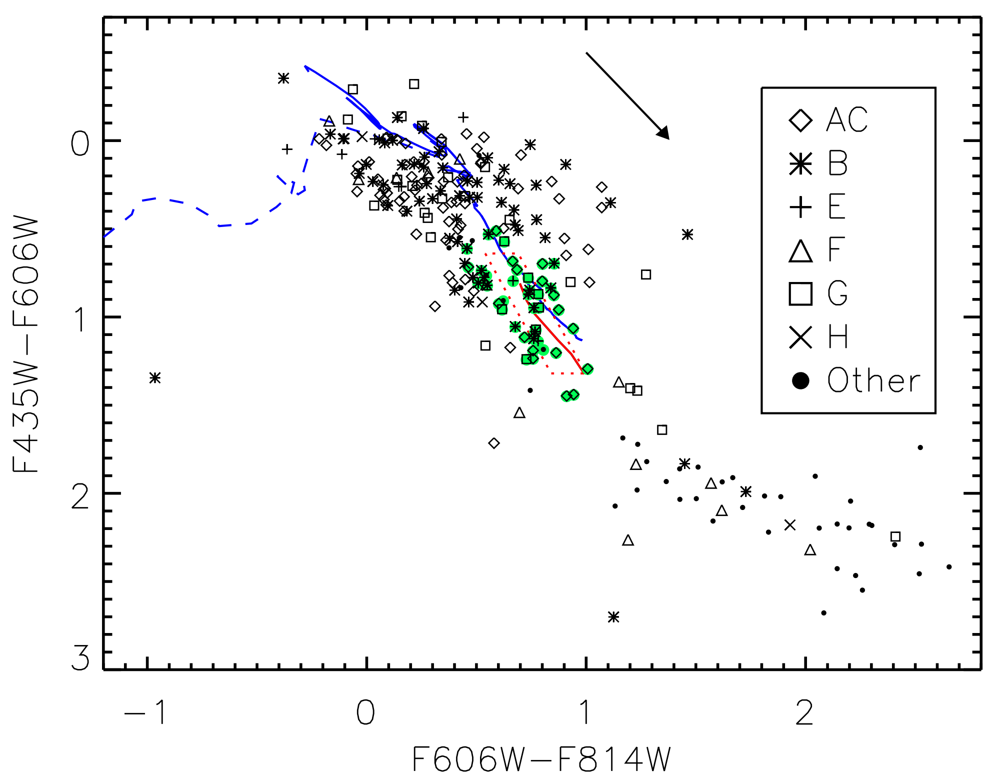

FIG. 9.— Color-color diagram for all point sources with 20 $< V_{606} <$ 26. The red dotted region denotes the expected colors for Milky Way globular clusters based on the Harris (1996) catalog; see §3.4 for details. The solid, red line within the detection region shows the predicted colors for old stellar populations from the simple stellar population models of Maraston (2005). Black symbols indicate the regions where the point sources are located (see legend for key); green circles underlie those objects whose photometric error ellipses intersected the GC selection region. For reference, the nebular (blue, dashed) and normal (blue, solid) evolutionary tracks as described in §2.4 and an A_{606}=1 reddening vector are overplotted as well.

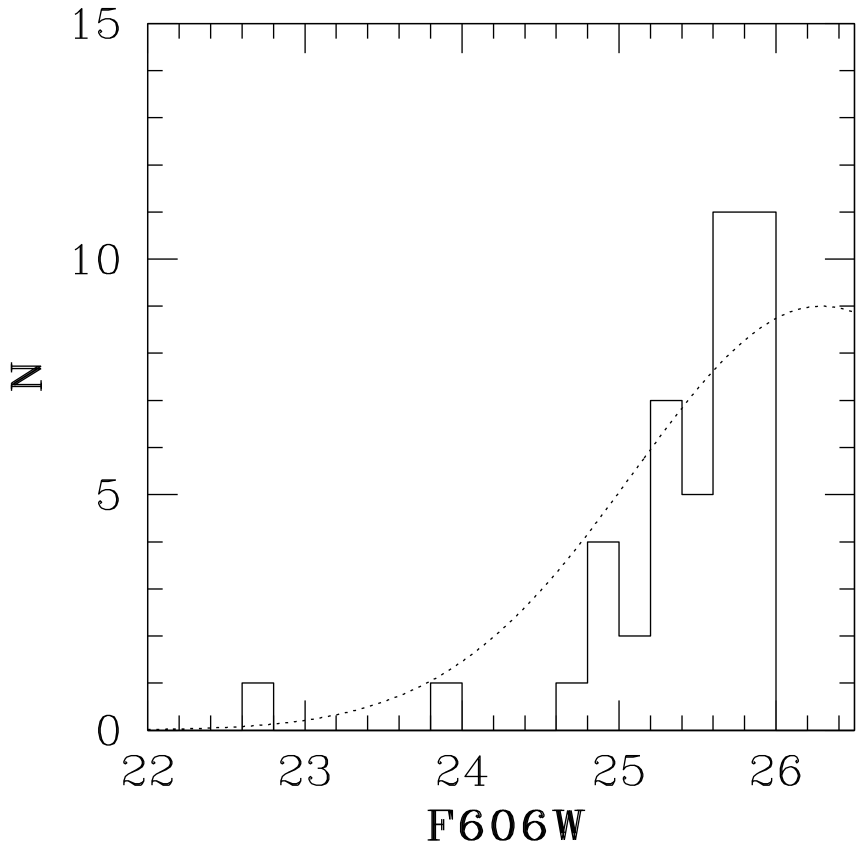

FIG. 10.— Raw V_{606} luminosity function (histogram) for all GC candidates with no correction made for any (small) background contamination or for photometric completeness. The dotted line shows the expected luminosity function for GCs located at the distance of HCG 31: a peak magnitude of $V_{606} = 26.3$ (corresponding to $M_V = -7.4$) and a dispersion of $\sigma = 1.2$. The plotted function is *not* a fit to the histogram, but is shown to indicate the shape of the function.

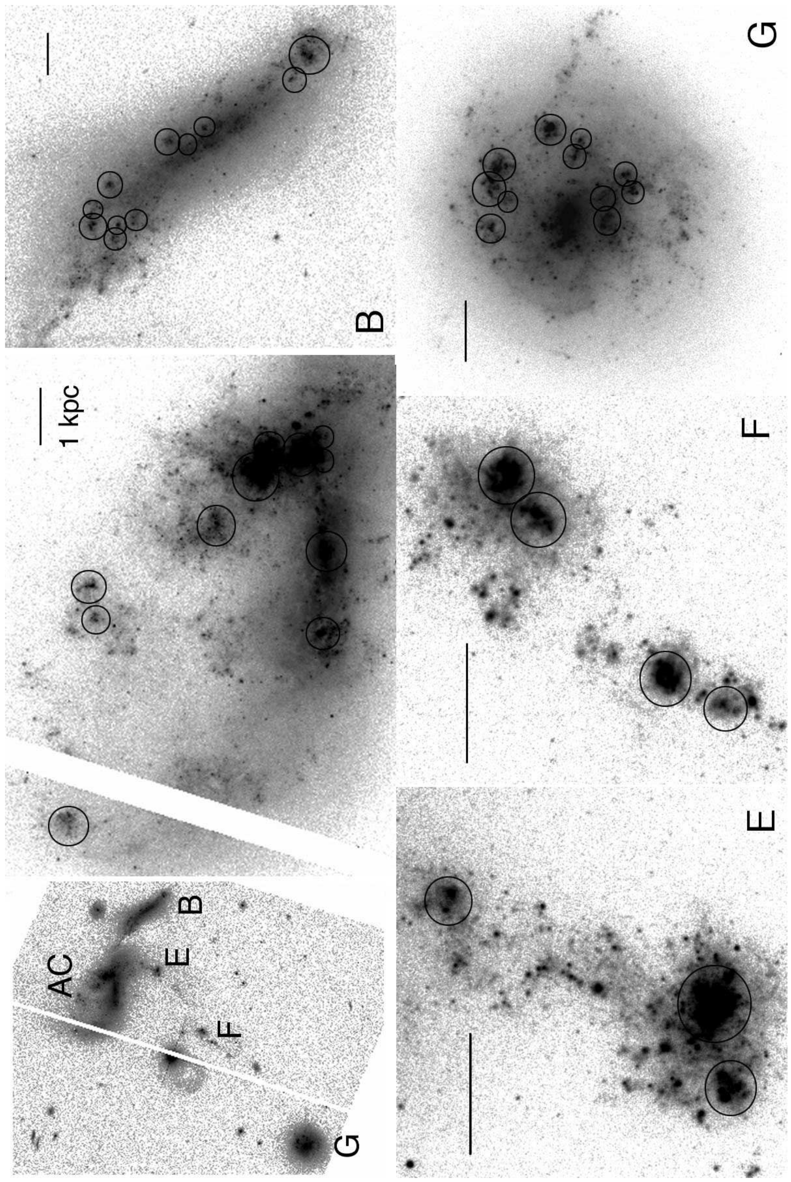

Fig. 11.— Star-forming complexes are shown in the composite logarithmic grayscale image of HCG 31. The whole field is shown in the top left, with the galaxies and tidal structures labeled. Close-ups of each region are shown in subsequent frames. Measured complexes are indicated by solid, black circles; note that these complexes may encompass several star clusters. The line in each grayscale image represents 1 kpc. (● This figure will be replaced with a 3-color *HST* image.)

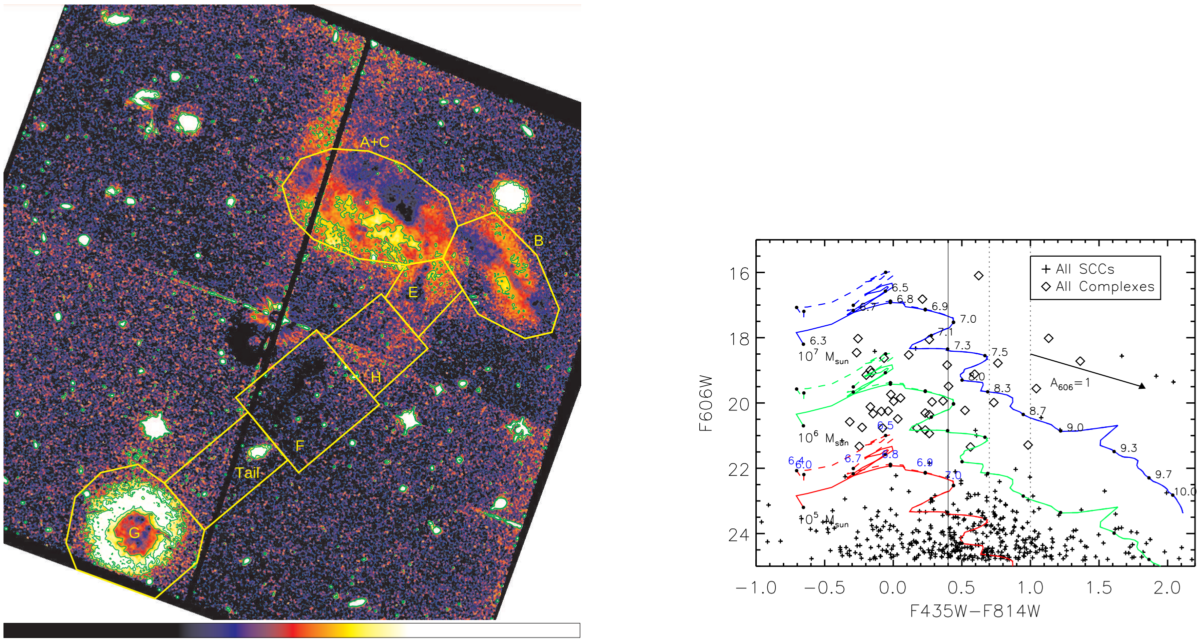

Fig. 12.— (*Left:*) A Vega-magnitude calibrated, point-source subtracted, boxcar smoothed (with a 13 pix window), B_{435}–I_{814} image of HCG 31. The image has been corrected for Galactic extinction. The scale is linear, and plotted colors range from −0.9 (black) to 1.9 (white). The blue-red transition occurs at B_{435}–I_{814}=0.4, and B_{435}–I_{814}=0.7 and 1.0 contours are plotted in green. Regions are labeled as in Figure 2. The lack of red in much of the F region indicates that there is no evidence for an older stellar population in the diffuse emission in that region. In contrast, the tidal material pulled out to the north of A+C and coincident with E and H clearly has redder colors (B_{435}–I_{814}=0.4–0.9). (*Right:*) V_{606} vs. B_{435}–I_{814} color-magnitude diagram of the SC candidates and complexes; symbols and tracks are as described in the caption to Figure 5. The vertical lines at B_{435}–I_{814}=0.4, 0.7, and 1.0 mark the blue-red transition, and the green contour levels in the left hand image.